ENSO simulated with Intermediate Coupled Models and evaluated with observations over 1970-1996. Part I : Role of the off-equatorial variability

by

C. Perigaud, F. Melin, C. Cassou

submitted to Journal of Climate

June 26, 1998

Jet Propulsion Laboratory, MS 300/323, 4800 Oak Grove Dr., Pasadena, CA 91109.

email=cp@pacific.jpl.nasa.gov

Off. Equatorial Variability

Abstract

ENSO simulations are investigated in 30 year integrations of various Intermediate Coupled Models and compared with observed SST, wind and thermocline depth anomalies over the tropical Pacific. The Cane and Zebiak's model simulates warm events with a period close to the observations, but with westerlies that are located 30° east of them and thermocline anomalies in the western Pacific that are much shallower. Between two warm events, the model simulates a series of three weak and short cold SST peaks and hardly ever simulates easterlies. The SST in the eastern equatorial Pacific is not sensitive to thermocline depth anomalies, but to the anomalous downwelling of surface currents induced by Ekman shear. The model simulates a pair of very strong cyclonic wind stress curl anomalies on both sides of the equator in the eastern off-equatorial domain between 7° and 15° of latitude. These are necessary to maintain the oscillatory regime. So are the ocean meridional Rossby modes higher than 5. The thermocline zonal slopes required to balance the off-equatorial curl anomalies are about three times steeper than the ones required to balance the zonal stress along the equator and the excess of zonal pressure gradient exerted by the off-equatorial coupled system plays a crucial role in reversing and triggering the growing events. Six months after the warm peaks, the whole ocean between 15°S and 15°N is significantly upwelled. The equatorial oceanic heat content is recharged by the South prior to a warm event .

Conversely to simulations when the model is driven by observed wind anomalies, increasing the friction in the baroclinic ocean does not decrease the off-equatorial variability, but significantly alters the low-frequency oscillations that are no longer ENSO-like. Introducing the parameterization of subsurface temperature derived from hydrographic profiles in the ocean component, does not allow the coupled model to recover cold events as in a forced context. Introducing the parameterization of convection derived from high cloud temperature measurements allows the model to better locate the wind anomalies, but the bias towards equatorial westerlies and upwelled ocean is also significant in this case.

Thus modifying the ocean component only or the atmosphere only does not have the same impact on simulations as in a forced context. The coupling allows new mechanisms to grow and govern the model behavior. One of them is the slow meridional oceanic mass adjusment in zonal quasi-equilibrium with the winds.

1. Introduction

Today understanding El Niño and being able to predict it one year in advance, is still a big challenge. Besides understanding why the ocean-atmosphere system has an oscillatory behavior, a lot of detailed questions need to be answered in order to improve the predictive skill of models. For example, the questions "Why are some warm events stronger than others?", or "Why do some last longer?", or "Why do some decay back to normal conditions and others reverse to cold events?" are as important as "What is a warm event triggered by ?". One difficulty to keep in mind is that the explanations are probably specific to each event, and even for a given event, the answer is a combination of various mechanisms in the ocean atmosphere system. Compared to the simplified physics simulated by Intermediate Coupled Models (ICM) such as the ones described in Cane et al (1986), Battisti (1988) or Kleeman (1993), many more processes are involved in reality. Nevertheless, if an ICM does simulate realistic oceanic and atmospheric fields, it is worth using it as a tool to address some of these questions. Prescribing the climatology in ICMs that are anomaly models, can be viewed as a big advantage because the climatology then represents fairly well the reality. Simulations are not subject to major problems of climate drifts as in more complex models. It is common to hear that anomaly models cannot provide any valuable insight on ENSO because most of the processes involved in the latter, like transports by currents or air-sea fluxes require the total fields and not the anomalies only. It is thus worth recalling that anomaly models do involve the full fields. Equations are obtained by decomposing the various fields into a climatological and an anomalous part. There is no assumption about the anomalous part being small relative to climatology. The

nonlinear terms are certainly retained in the anomaly model. Indeed they are a subject of particular attention in this study. As ICMs are based on simplified physics, the vertical mixing in the upper ocean, the atmospheric convection have to be parameterized. Parameterizations certainly cannot accurately reproduce the mechanisms at work in Nature, but if their estimation is accomplished via analysis of observations, they are representative of the reality to some extent. As more and more data are available, it is worth using them to improve these estimations and benefit from the advantages of ICMs to learn more about coupled modeling of ENSO. The understanding of model coupled behavior is still very premature in comparison to ocean models forced by prescribed atmospheric conditions or to atmospheric models forced by precribed SST. A better understanding of the mechanisms involved in the oscillatory behavior and a better knowledge of the spatio-temporal features of the various fields are essential to evaluate the extent to which one can trust what a model predicts.

The present study starts with the Cane and Zebiak's model (Zebiak and Cane, 1987), hereafter named CZ. The code, input files (parameters, climatological fields, wind stress anomalies used for initialization) as well as the initializing and coupling procedures, were all kindly provided by Dr Zebiak from Lamont Doherty Earth Observatory (LDEO). Various data sets have been used to validate the model when it is forced by observed wind anomalies (Perigaud and Dewitte, 1996) and to derive new parameterizations (Dewitte and Perigaud, 1996; hereafter named DP96). In DP96, the latter are introduced in the model, and lead to more realistic oceanic and atmospheric fields. However, DP96 is limited to experiments where the model is run in a "forced" context, meaning either the ocean model forced by observed winds drives the atmosphere without feedback to the ocean, or vice versa the atmosphere forced by observed SST drives the ocean. By opposition, the present study is devoted to experiments where the model is run in a "coupled" context, meaning both the ocean and the atmosphere are driven by the simulated wind and SST respectively, none of the model components being ever constrained by data. An integration over thirty

years is the minimum duration of the coupled simulations presented in this study. Observed SST and wind since 1970 and oceanic heat content since 1980 are used to evaluate the model outputs over the Pacific between 15°S and 15°N.

The three major modifications proposed in DP96 consist in changing the subsurface temperature parameterization by the one derived from hydrographic profiles, replacing the iterative convergence scheme of the atmosphere by a parameterization of the heat released by convection derived from high cloud convection and SST data, and increasing the friction in the ocean baroclinic model to better fit observed sea level and zonal current anomalies. Throughout this paper, these three modifications will be respectively refered to with the words "Tsub", "Conv" or "Fric" for conveniency. In order to understand their impact on the model coupled behavior, one first needs to thoroughly analyze the CZ model with its standard parameterization. Particular attention is paid to the mechanisms simulated in a coupled context, because they are very different from the ones simulated in a forced context. Thus important differences found outside the equatorial band appeal for testing the role of the off-equatorial variability in the coupled behavior. Throughout this paper, the equatorial band designs the latitudes between 5°S and 5°N, and the off-equator between 7° and 15°. According to the "delayed oscillator" and illustrated by Battisti (1989), the off-equatorial variability is not involved in the coupled behavior. But this is not the case for the "recharge oscillator paradigm" proposed by (Jin, 1997ab) and illustrated with the CZ model.

Part I of this study is devoted to the CZ model with its standard parameterization and to the impact of the three modifications proposed in DP96 when they are implemented one at a time. Part II is devoted to the impact of the combined three changes, and to the replacement of the atmospheric model with a statistical one. Although all the ICMs presented in this study assume similar physics, they have very different coupled behaviors. The models described subsequently are called by a compound

"ocean.atmosphere" name which specifies the changes applied in each component in comparison with the CZ model.

Part I is organized as follows. Section 2 presents the datasets. The fields simulated by CZ are compared with observations in Section 3. Experiments testing the role of the off-equatorial variability on the coupled behavior are presented in Section 4. The equatorial and off-equatorial coupled mechanisms involved in the oscillations simulated by CZ are analyzed in Section 5. The impacts of applying either Fric, or Tsub or Conv on the coupled behavior are described in Section 6. A summary of results and their consequences for Part II are proposed in the last Section.

2. Data

Observed SST, wind stress and thermocline depth anomalies are used in this paper to validate simulations. In addition, SST and winds are used to initialize the coupled models and to replace the atmospheric component by a statistical approach (see Part II). For commodity, all the datasets have been monthly averaged and interpolated on the atmospheric grid of the CZ model (5°.625 in longitude and 2° in latitude).

The SST anomalies are derived either from the CAC data set provided by the website http://ingrid.ldgo.columbia.edu/SOURCES/.CAC/.sst/, or from the Reynolds and Smith (1994) data set between November 1981 and December 1994 and completed over 1980-1981 with surface temperatures measured by XBT data as described in Perigaud and Dewitte (1996). The CAC data set is routinely used by the LDEO group for validating the ENSO forecasts (i.e. NOAA Climate Diagnostics bulletins) and covers a longer period back since January 1970. For both data sets, anomalies are computed relative to the climatology covering as many complete years as possible. The CAC and Reynolds anomalies averaged over Niño3 (5°S-5°N, 90°W-150°W) are compared in Fig. 1a. Their difference can be as large as 1°C like in 1989. Variability maps (Fig. 2ab) show that most of the SST signal is located in the eastern equatorial Pacific with two local maxima, one

along the Peruvian coast and one offshore located at 110°W-1°S. Compared to CAC data, the Reynolds data have a signal more confined to the equator and an off-shore maximum almost as strong as the coastal one. Comparing the total signals indicates that the discrepancy is not only due to the difference in climatological reference. It is also related to data uncertainty. Unless specified otherwise, it is chosen to use the CAC data for model evaluation because of its longer coverage in time.

The wind stress anomalies are either the pseudo-stress data provided by Florida State University (see Goldenberg and O'Brien, 1981) or the "detrended" data provided by Dr S. Zebiak from LDEO. The former are named "non-detrended" in this paper. The latter are available since January 1964 and are regularly updated by LDEO after applying a detrending and smoothing filter on the non-detrended data since 1960 (see Cane et al, 1986). The discrepancy between the two data sets is partly due to a difference in wind measurements that shifted from wave height estimates in the 70-s progressively to anemometers in the 80-s, and partly due to actual wind variability. Both data sets are used in this study. Pseudo-stress are converted into stress with a drag equal to 2.00×10^{-3}, which corresponds to the one used by the LDEO to get the initial conditions of the CZ model for the forecasts published in the Climate Diagnostic bulletins. The zonal wind stress anomalies averaged over Niño4 (5°S-5°N, 160°E-150°W) are compared in Fig. 1b. Their difference can be as big as a wind change during an El Niño event. It reaches 0.2 Dyn/cm^2 between 1973 and 1976 or in 1992-1994. Forecasts are expected to be highly sensitive to the choice of the wind used to initialize the model. Conversely, it is not known if the behavior of an ocean model coupled to a statistical atmosphere during decade-long simulations is highly sensitive or not to the choice of the data used to build the statistical atmosphere itself. Indeed the interannual events observed by both data sets are very similar. Time series are highly correlated (0.86), the timing of the peaks and duration of the ENSO events are the same and the discrepancy is mostly a decadal trend. The variability maps have very similar patterns. Except in Part II where both wind (and SST)

data sets are tested in experiments with the statistical atmosphere, choice is made hereafter to use the detrended wind data set to evaluate how the coupled model compares with observations.

The variability of the zonal wind component has a maximum located close to the dateline (Fig. 2c). Most of the variability of the meridional wind stress anomaly (Fig. 2d) is located along the climatological wind convergence zones. Although the anomalous meridional wind has little impact in driving baroclinic anomalies along the equator, it deserves more attention as it drives surface convergence along the ITCZ during warm events (Deser and Wallace, 1990).

Thermocline depth anomalies are estimated either from the ocean heat content in the upper 400 meters named "T400", or from the depth of the 20° isotherms named "D20", as described in Perigaud and Dewitte (1996). Both data sets covering January 1980 to August 1994 were provided by Dr N. Smith from Bureau of Meteorology Research Centre (see Smith et al, 1995). Both are used because neither D20 nor T400 is an exact representation of the thermocline depth, and their discrepancy can provide an order of magnitude of the data uncertainty. As expected, the biggest difference between the two signals is found in the cold tongue in the eastern Pacific, but averaged over Niño3, the time series agree within 3 meter rms difference over 1980-1994, with a maximum difference of 8 m in 1983 (Fig1c). T400 or D20 averaged over the northwestern (130°E-160°E / 3°N-9°N), or southwestern (140°E-170°E / 3°S-9°S) region agree very well with a correlation larger than 0.95 and an rms difference smaller than 1m, in the north as well as in the south. For a given data set, the difference between the North and the South are more significant. Southern and Northern time series are correlated by 0.81. More details about the asymmetry between the North and the South are given in Part II. For simplicity, the authors define here a NiñoW index, which is the average of the thermocline anomalies over the region (130°E-170°E, 9°S-9°N). Observed indices are presented in Figure 1d. As expected, warm (cold) events correspond to shallow (deep) thermocline anomalies in the

West of the order of 20 to 30m. It is worth remembering that thermocline displacements in NiñoW have an amplitude similar to that observed in Niño3. Variability maps are similar for both estimates, with maxima along the equator east of the dateline and in the western Pacific on both sides of the equator (Fig. 2e). It is equally justified to use T400 or D20 for evaluating the model simulations. Unless specified like in Part II, T400 is used in the rest of the paper.

Oceanic and atmospheric fields vary together in time and one expect warm SST peaks associated with downwelled thermocline in the East, westerlies in the Central Pacific, southerlies along the ITCZ and upwelled thermocline in the West. But for prediction purposes, it is important to capture the phase shifts that may occur between the various fields. A striking one is that the peaks of westerlies lead the warm peaks by a couple of months. Statistically over 1970-1996, the Niño4 wind index is correlated to the Niño3 SST index by 0.71. The correlation increases up to 0.78 when a 3-month lead is introduced in the wind series, whereas it drops to 0.48 with a 3-month lag. Statistically over the period 1980-1995, the Niño3 H series are best correlated with the Niño4 TX index without any phase shift (0.85). They slightly lead the Niño3 SST series, correlation increases from 0.78 to 0.83 when a 2-month lead has been introduced in the thermocline series whereas it drops to 0.61 with a 2 month lag. As expected the NiñoW thermocline is phase-shifted with the Niño3 SST, but depending on the period which is considered, it can be late or in advance. Thermocline shoalings in the west in 1983, 1987, and 1992 all lag the SST warm peak. The downwelling in 1989 is also a consequence of the cold event. The downwelling in 1985-1986 can rather be viewed as an example of oceanic heat content accumulation in the western Pacific prior to the 1987 El Niño, that follows the scenario proposed by Wyrtki (1985).

3. Comparison with the CZ standard coupled simulations

The CZ model is known for its skill to simulate interannual events that agree reasonably well with reality. As illustrated in Figure3a, it simulates warm events that have a period close to 4 years, present some irregularity and are phase-locked with the seasonal cycle. The oscillatory behavior is indeed very irregular past year 30 (not shown), the model simulates very weak fluctuations between year 40 and 60 followed by another serie of strong ENSO-active period during 30 years. So the index simulated by the experiment described here has the same characteristics as the ones presented in Zebiak and Cane (1987). The two simulations are not identical though because they have different initial conditions. Because of ENSO forecasting issues addressed in a study following this one, the simulation is initialized with the oceanic and atmospheric conditions obtained by forcing the CZ ocean component with the detrended wind stress anomalies from rest since January 1964. This corresponds to the standard procedure applied for initializing the forecasts. It also corresponds to the "Control Run" examined in DP96. Except for a few test experiments that are specified below, the coupled simulations presented in this paper are initialized with the fields provided by the "Control Run" in January 1989. This choice is arbitrary and is retained here only for simplicity.

The simulation analyzed in this section is referenced as CZ (run1a). Reproducing a realistic period of oscillations is only one aspect of the model skill in reproducing realistic ENSO signals. The amplitude of the SST, wind and thermocline anomalies and the phase shifts between these signals are crucial. The amplitude of the warm SST peak is about twice larger than the observed one (Fig. 3a). Because coupled models have a nonlinear behavior, it is not straighforward to reduce the amplitude of the SST as it is in a forced context for example by decreasing the drag coefficient. Note that the drag coefficient used in the CZ model when it is run in a coupled context is equal to 3.29×10^{-3}. This is 1.645 times larger than the drag used in the forced "control run".

Although the amplitude of the SST Niño3 index is too large, the westerlies averaged over Niño4 have an intensity similar to the observed one (Fig. 3b). The wind index is positively correlated with the SST index by 0.90. Conversely to observations, the wind is not leading the SST signal, but actually slightly lagging it. The correlation increases to 0.93 with a 1 month lag introduced in the wind and stays at 0.90 with a 2 month lag whereas it drops to 0.76 with a 2 month lead. This happens because the atmosphere model is not a "slave" model, the time lag is introduced in solving the iterative convergence scheme of the atmosphere that is initiated with the wind stress anomaly at the previous time step. Another striking feature is that the model hardly ever reproduces easterlies. Even when the SST index is negative, the wind never blows westward for more than a few months in a row, it reverses every 9 months from mild easterlies to mild westerlies. It is interesting to remind that forced by observed winds over 1980-1993, the simulated SST and wind indices are never below -0.6°C and -0.1 Dyn/cm^2, whereas the ocean model with the new Tsub parameterization recovers cold temperatures and easterlies of -1.8°C and -0.4 Dyn/cm2 in 1988 (DP96). Section 6 examines if this improvement holds in a coupled context.

In the eastern Pacific, the simulated thermocline anomalies (Fig. 3c) have an amplitude close to the observations. During interevents, they present large fluctuations that are not found in observations. They are in phase with the wind. Correlation between thermocline displacements and SST time series in the East is 0.78. Introducing a lead or a lag between the two series decreases the correlation. The thermocline downwells by one month prior to the SST warming, but it stays deep as long as the westerlies blow, and it actually comes back to normal two months after the SST signal.

In the western Pacific (Fig3d), the simulated thermocline anomalies are way larger than in the east (note the change of vertical scale). Between year 10 and year 12.5, the thermocline changes by 94m. This is way bigger than the maximum change ever observed in reality (see Fig1d) or in the "control run " (extrema are +19m in 1988 and -30m in

January 1992). Anticorrelation between NiñoW H and Niño3 SST or Niño4 TX indices are respectively 0.71 and 0.75 and increases to 0.94 with a 2 month lead introduced in the SST and to 0.95 with a 4 months lead introduced in the wind. The strong thermocline shoalings in the west are clearly a consequence of the warming in the eastern Pacific. During interevents, the thermocline is subject to a series of 3 fluctuations every 9 months, together with zonal baroclinic current and wind stress reversals. These fluctuations correspond to the coupled "mobile mode" described in (Battisti and Mantua, 1995). Nine months is the time for a Kelvin wave followed by a first Rossby wave to cross the entire Pacific from the western to the eastern boundary and back to the western boundary. Such waves can complete 3 back and forth loops before being damped by a factor 2 with the weak friction assumed in CZ (the Rayleigh damping time is equal to 30 month). Nine-month baroclinic fluctuations are also found in experiments forced by observed winds and increasing the friction suppresses them as well as reduces the off-equatorial thermocline displacements to the observed level (see Perigaud and Dewitte, 1996). The impact of a stronger friction on the coupled behavior is examined in section 5. Besides the overly large amplitude of displacements and the brief fluctuations, the position of the thermocline averaged over the 30 years is not normal, but upwelled. Thus the anomaly model simulates coupled oscillations that have a mean state biased towards warm SST, westerlies and upwelled thermocline in the western basin. The 30-year mean Niño3 SST, Niño4 TX and NiñoW H indices are respectively 0.6°C, 0.13 Dyn/cm^2 and -20m.

Time series are useful to give some insight on this question, but box averages can be misleading and must be completed with variability maps. The SST patterns (Fig4a) are similar to the observations in location, but not in amplitude nor in meridional extension. The signal along the coast is much more displaced to the South than in reality, with strong anomalies extending South of 5°S and very weak anomalies North of 2°N.

The simulated zonal wind (Fig. 4b) has a maximum along the equator which is actually way stronger than in Nature. In addition, it is shifted by about 30° to the east.

Averaging over Niño4 region which is centered on the observed maximum variability is deceptive because it takes a lot of points with very low variability on the western side of the region that compensate for the very strong variability on the eastern side. In a forced context, the CZ model also simulates an eastward shift which is corrected by "Conv" (see DP96). The impact of this modification on the coupled behavior is examined in section 5. The large anomalies simulated in the eastern equatorial and off-equatorial domain correspond to strong easterlies during warm events. Along the equator, they have a negative coupled feedback on the system that needs to be compensated by the anomalous convergence of the meridional wind component, otherwise the model does not oscillate (Perigaud et al, 1997).

The meridional wind converges equatorward during warm events, but the strong anomalies are not located along the ITCZ nor the SPCZ as in reality, they are displaced way far in the eastern Pacific (Fig. 4c). The maximum in the Southeastern Pacific happens to be in a region of minimum observed variability. In addition, the Northern maximum is significantly displaced to the North.

The simulated thermocline depth (Fig. 4d) has a much stronger variability than observations everywhere, except between 100°W and 140°W at the equator. It is particularly large off-equator on the eastern and western sides of the basin. As there is no landmask in the model, the maximum in the Southwest is located to the West of the observed one. In addition, because this map does not account for the non-zero 30-year mean position of the thermocline, discrepancy is indeed particularly large in the western Pacific. Let us examine the anomalies simulated at a given time.

The most pronounced thermocline displacements happen past the warm peaks of the SST Niño3 index. The topography map presented in Figure 5a is the average depth anomaly between month 3 and 7 after the warm peak simulated in year 12 (it was checked that the same situation is reproduced after any other warm peak). For comparison with the model, the observed thermocline anomalies are averaged over January 1983 and May 1983.

This period corresponds to the strongest 5 month-averaged topography observed between 1980 and 1994. The observed map (Fig. 5b) presents some similarity with the model. The thermocline is downwelled in the equatorial eastern Pacific and upwelled in the Southwestern Pacific near the dateline by the same order of magnitude. But the simulated thermocline is downwelled by about 80m in the Northeast and upwelled by about 70 m west of the dateline in the North and the South, which is much larger than in reality.

Let us now consider the wind stress curl anomalies during warm events. As expected (Gill, 1980), the warm SST anomalies in the equatorial band generate a pair of cyclonic vortices north and south of the equator. This is reproduced by the model (Fig. 5c) and found in the observations to some extent (Fig. 5d). The observed cyclonic curl in the North is closer to the equator. Actually North of 5°N, the curl is anticyclonic, we come back on the latter in Part II. Here attention is paid to the difference in amplitude and position of the cyclonic pair. The simulated cyclonic curl extrema are located in the eastern Pacific beyond 9° of latitude, shifted by more than 50° in longitude and 5° in latitude. Even though it corresponds to the strongest observed signal, its amplitude is much weaker than the simulated curls. The latter are due to the zonal wind that reverses sign between 5° and 15°. This is not found in data.

It is interesting to compare the thermocline and the curl maps. According to Ekman pumping, one can expect significant thermocline displacements induced by such strong curls. Indeed for observations, the upwelled position of the thermocline at 170°W, 9°S three months after the warm peak, is consistent with the ocean response to a negative curl multiplied by the value of Coriolis at that latitude. But for the model, the downwelled position of the thermocline in the Southeastern Pacific is not. The model thermocline displacements are not governed by Ekman pumping, as explained in Section 5.

The CZ model has been designed for representing equatorial processes. Since the off-equatorial anomalies simulated in a forced context did not come out as a major deficiency in the validation studies and since coupled experiments reproduce a realistic

period of oscillation, little attention has been paid to the large thermocline and wind anomalies occuring off-equator in a coupled context. Whether they play a role in the model oscillatory regime or not, is tested in the following section.

4. Testing the role of the off-equatorial variability

The oscillatory nature of ENSO can theoretically be reproduced by equatorial processes only (i.e. Schopf and Suarez, 1988). Indeed anomalies observed in the equatorial Pacific are explained to a large extent by equatorial wave reflection (i.e. Mantua and Battisti, 1994; Boulanger and Fu, 1996). Nevertheless, it is quite possible that equatorial processes are not sufficient to sustain the oscillations and that the off-equatorial thermocline displacements observed in the western Pacific play an important role (Wyrtki, 1985; White et al, 1989). The authors surely do not want to feed this controversy by providing general statements about what happens in reality. Their objective in this paper is limited to the understanding of the coupled behavior of the CZ model. Results obtained with the ICM presented in (Battisti, 1989) show that the role of the wind beyond 5° of latitude is negligible and that the oscillations are due to the Kelvin and first gravest meridional Rossby modes. Experiments are performed below to test if this is the case for the CZ model.

a) Filtering out the off-equatorial winds

The model is run with its standard parameterization while the off-equatorial winds are filtered out like in Battisti (1989) in an experiment named (run 1b). At each time step of the simulation, the wind stress anomalies are multiplied by a filter equal to 1 between 5°S and 5°N, 0 beyond 9°S and 9°N and linearly decreasing from 1 to 0 between 5° and 9°. As the model without filter simulates zonal wind anomalies that decrease between 5° and 9° and increase beyond, such a filter does not alter too much the curl in the 5°-9° band while it allows to filter out the strong off-equatorial curl anomalies. Experiment 1b (Fig. 6a) shows that after one oscillation, the index reaches a permanent slightly cold state that lasts for 20

years without warm events. Because of these unexpected results, several other experiments were performed to examine the validity of this test. Various initial conditions were used, testing stronger initial anomalies (January 1983 or May 1988 of the "Control Run") or applying "initial wind kicks" as in Zebiak and Cane (1987). Being aware that the filter does create some fake curl in the 5°-9° band, we tested various filters that are smoother. Experiments were run with linear decrease applied over a wider band of latitude (5°-15°) or with Gaussian decays beyond 5° of latitude with half-decay at 11°. Whatever the filter, whatever the initial conditions, the CZ model does not sustain oscillations anymore. The simulated signal is damped after one or a couple of oscillations at best. So the off-equatorial wind anomalies in the CZ model play a crucial role to sustain the oscillatory behavior. This conclusion illustrates the fact that our understanding of the physical processes involved in ENSO does not depend only on the basic physics assumed in the model. Although the Battisti (1989) and CZ models are both anomaly models based on the same physics, differences in the parameterizations, the numerical schemes, the climatological fields prescribed in the two models lead to distinct coupled behaviors as thoroughly described in (Mantua and Battisti, 1995). The present experiments illustrate an additional particularity. Battisti's model works as a "delayed oscillator" whereas the CZ model does not.

How the off-equatorial winds alter the coupled regime is now examined. The winds induce SST changes either via the baroclinic fields or via the Ekman currents. In (run 1b), the wind stress anomaly is filtered prior to time-stepping both the Ekman and the baroclinic model components. The filter is now applied prior to time-stepping the mixed-layer model only (run 1c). The oscillatory behavior of the model is then similar to the standard one (Compare the dotted line of Fig. 6a with Fig. 3a). Therefore the role of the off-equatorial winds in driving Ekman currents is not critical. When the filter is applied prior to time-stepping the baroclinic model only (run 1d), the index does oscillate for a couple of cycles initially, but eventually reaches a permanent slightly warm state (Fig. 6a

thin line). Thus the off-equatorial winds contribute to maintain the oscillations mostly via the baroclinic ocean.

b) Filtering out the off-equatorial baroclinic ocean

Next the baroclinic signal simulated in (run 1a) is decomposed into Kelvin and Rossby modes and additional experiments are done to examine the role of these modes in maintaining an oscillatory regime. The baroclinic fields simulated in (run 1a) are projected on the Kelvin and meridional Rossby modes up to 20 as in Battisti (1989). Similarly to the results of this paper, the highest modes are found in the eastern Pacific. Because the signal reconstructed with only the first gravest Rossby mode and the Kelvin mode explains more than 95% of the thermocline variance in the 5°S-5°N band, the oscillatory behavior of the model is considered as sustained by these two modes only. Indeed the high Rossby modes in the eastern Pacific are not expected to influence the oscillatory behavior of the model because they are damped before they reach the western boundary: free Rossby waves for modes higher than the fifth one, propagate slower than 25 cm/s and cross the Pacific from the eastern to the western boundary in more than 4 years. However this argument does not imply that high Rossby modes do not play a role. First thermocline anomalies are not free to propagate when they are associated with wind anomalies in coupled models. Second they may contribute to the oscillatory regime without explicit reflection at the boundary. It has actually never been demonstrated whether they contribute or not.

Various experiments retaining only the gravest modes have been performed to test their role in the interior domain or by their reflection at the meridional boundaries. Two are presented in Figure 6b. The first one allows only the 5 gravest Rossby modes to reflect into Kelvin waves at the western boundary (run 1e). The second one consists in reflecting the Kelvin wave into the 5 gravest Rossby modes only at the eastern boundary (run 1f). In the former, the model fluctuations are damped to zero past a couple of oscillations. In the latter, the model reaches a warm state past 10 years. Both experiments indicate that the Rossby modes higher than 5 are necessary to sustain the oscillatory regime for the CZ

model. Performing different tests on the number of modes retained at the eastern or western boundary confirm this result: a wide variety of responses (damped, sub-annual oscillations or decadal trend) is found, but whatever the case, the model behavior is severely affected.

Indeed the importance of the off-equatorial ocean has been highlighted by Cane and Zebiak (1985), Cane (1992) and with a conceptual model (Jin, 1997a) or a CZ-type stripped-down model (Jin, 1997b). The present results show that high Rossby modes reflect at the meridional boundaries and that explicit reflection is necessary for oscillations. This does not mean that these modes do not play a role in the interior domain. Indeed experiments where the high modes are filtered in the interior domain have been performed. They show that the behavior is drastically affected by the high modes in the interior. Experiments where the wind is not filtered by projection on the baroclinic modes retained for the ocean develop strong wind curls when the first warm peak grows that are associated with high baroclinic ocean modes and filtering them out significantly modifies the current anomalies in the equatorial band. As a consequence, the model integration cannot be achieved without violating the stability criteria in time-stepping the SST equation. This test is meaningful. The numerical instability is not at all due to errors in the projection into Rossby modes and reconstruction of the fields. It was verified that the sum of the first 20 Rossby modes reconstruct perfectly well the thermocline and baroclinic current anomalies at any time. This test illustrates that the high Rossby modes also play a strong role in the coupled behavior via the interior of the domain.

The reader should be aware that the role of the off-equator is big only when the CZ model is run in a coupled context. When the model is forced by observed winds (run0), the same filtering tests have very little impact on the SST (Fig. 6c). The experiment (run 0b), where the wind stress anomalies are filtered out as in (run 1b) simulates SST anomalies in very good agreement with the "control run" (run 0a). So does the experiment (run 0c), where only the 5 gravest Rossby modes of the baroclinic fields are retained in the

whole domain of the baroclinic ocean model. Changes are of course even smaller when the modes are filtered only at the meridional boundaries like in run 1e or 1f.

5. Analysis of the equatorial and off-equatorial coupled mechanisms

The coupling between the baroclinic ocean, the mixed layer and the atmosphere can be understood by examining the various terms involved in the SST equation. The temperature rate of change $\partial T/\partial t$ is the sum of 7 terms that are described by the following equation, named Eq T:

$$\partial T/\partial t = - U \times (\underline{T} + T)_x \quad (T1)$$

$$+ \underline{U} \times (T)_x \quad (T2)$$

$$- V \times (\underline{T} + T)_y \quad (T3)$$

$$+ \underline{V} \times (T)_y \quad (T4)$$

$$- \gamma_1 \{M(WT) - M(\underline{W})\} \times \underline{T}_z \quad (T5)$$

$$- \gamma 2\, M(WT) \times (T - Tsub)/H1 \quad (T6)$$

$$- \alpha\, T \quad (T7) \quad :Eq\ T$$

Underlined variables correspond to the climatological fields. M(x) is the function M(x)=x if x positive and M(x)=0 if x negative. WT is the total upwelling rate at the base of the mixed layer, which is the sum of the anomalous upwelling W and the climatological upwelling $\underline{W}$. Terms T1 and T3 represent the horizontal advection by the anomalous currents in the mixed layer, U and V, that include the baroclinic components and the Ekman shear. Terms T2 and T4 correspond to the advection of anomalous temperature by the climatological horizontal currents. Term T5 represents the anomalous advection of cold waters from the base of the mixed layer due to a change in upwelling rate W relative to the climatological upwelling. Term T6 takes into account the thermocline influence on the subsurface temperature which is advected by the total upwelling.

The budgets simulated by run 1a are examined. The contribution of horizontal advection (terms T1 to T4) and vertical advection (terms T5 and T6) in the SST variations

highly depends on the location. Beyond 5° of latitude, the changes are explained by anomalous heat export by the climatological Ekman current divergence away from the equator (term T4). The other 6 terms are negligible. Note that the thermocline does not cool down the SST although it is very close to the surface in the western Pacific during warm events. The CZ model does not reproduce the western Pacific oscillator paradigm proposed in Weisberg and Wang (1997). The downwelled thermocline in the eastern Pacific during warm events does not either warm up the off-equatorial SST. These results are consistent with experiments (1bcd), the off-equatorial winds do not have a local impact on the SST via the mixed layer, they have an impact on the coupled behavior of the system via the baroclinic ocean. The off-equatorial wind anomalies are associated with the SST gradients. These are mostly governed by the equatorial SST variations.

a) analysis of the equatorial coupling

As distance to the equator decreases, more and more terms are involved in the SST budgets. It is important to separate behaviors slightly north of the equator from south of it, because neither the simulated anomalous fields nor the prescribed climatology are symmetric with respect to the equator. The SST anomaly at 5°S is twice larger than the anomaly at 5°N. The heating at 5°N is due to the equatorial anomalous heat source (term T4) as above, whereas at 5°S it is explained by the southward baroclinic current (term T3) that transports heat from the equator to the south. The source of heat here is the climatological background which is warmer at the equator than at 5°S because of the cold tongue extension South of the equator along the Peruvian coast. Experiments where the off-equatorial SST is filtered (not shown), demonstrate that this source is also necessary to sustain the coupled oscillations. Filtering the SST out in the North only has very little impact, while filtering it in the South only maintains the fluctuations within +/- 0.1°C during the 30 years.

The coupling along the equator is quite different. Zonal and vertical transports play the dominant role there. Results are presented in Figure 7 for the two terms of vertical

advection and for the sum of the 4 horizontal advection terms. They are compared to the local change corrected by the damping (term T7) in order to account for the phase lag introduced by the latter. Everywhere and always, term T5 helps the anomalies grow, it has a positive coupled feedback on the system. During a warm (cold) event, it has a warming (cooling) impact because the equatorial westerlies (easterlies) induce local downwelling (upwelling) by driving Ekman surface currents that converge (diverge). It is not leading the SST changes though. It is lagging them, except for the cold events in the central Pacific where signals are in phase.

In the western and central Pacific (Fig. 7ab), term T6 is competing term T5. Leading the decays of events (warm or cold) in the Central Pacific, it is responsible for reversing the SST trends. The thermocline there has a negative feedback on the coupled system. The impact of term T6 is not symmetric however with respect to the sign of the event. During cold events, weak downwelled thermocline anomalies are very effective to heat the system and erode the growing cold events, because the weak easterlies induce a local Ekman divergence that adds up to the climatological upwelling rate to advect the warm subsurface temperature anomaly. Conversely, a shallow thermocline is less efficient in eroding the growing warm events, because Tsub is not much sensitive to upwelled thermocline anomalies, and also because the cold thermal gradient anomaly is advected to the surface at a reduced upwelling rate. This is why warm events are so big compared to the weak and brief cold peaks.

In the eastern Pacific (Fig. 7c), term T6 presents unexpected features. The fact that the downwelled thermocline in case of warm events has a very little warming impact is due to the reduction of the total upwelling rate. But in case of upwelled thermocline (cold event), term T6 does not have a cooling impact, but a warming one. This happens because the (SST-Tsub) anomaly is negative, meaning that the cold subsurface anomaly due to upwelled thermocline is weaker than the cold surface anomaly. Thus term T6 in the eastern Pacific almost always contributes to heat up the system. This important result does not

correspond to expectations. Observations indicate that subsurface temperature changes are always bigger than the surface ones.

Horizontal advection helps the growth of SST anomalies, whether they are warm or cold. However mechanisms involved during warm events are quite different from cold ones. For warm events, horizontal advection is big over the eastern and central Pacific (Fig. 7bc) and term T4 is the dominant term among the 4 horizontal transports, i.e. the heating is due to the strong warm SST anomaly that is located South of the equator and that is advected by the climatological meridional current that flows northward at the equator. Term T4 leads term T5, but it does not either lead the SST changes. It was also tested if the reversal of the warming growth has a climatological origin such as the decrease of the prescribed currents (term T4) with the season in Spring. Based on experiments run with the climatological fields that are not monthly varying (either yearly averaged or fixed to a particular month), this is not the case. For cold events, the impact of horizontal advection is big over the western and central Pacific (Fig7ab), but it is then term T1 which is the dominant horizontal transport, i.e. the cooling is due to the zonal transport of cold waters from the central Pacific to the warm pool by the baroclinic westward anomalous current. Terms T1 and T5 are in phase at the cold peaks in the Central Pacific. Refering to Neelin (1991)'s description, the CZ model simulates warm states during which the "slow SST mode" is the dominant mode of variations, in contrast with cold events dominated by "fast baroclinic coupled modes".

b) Analysis of the coupling between the off-equator and the equator

As explained above, the thermocline anomalies in the central and western equatorial Pacific compete the growing cold events due to (term T5+term T1) or the growing warm events due to (term T5+term T4). If the equator is not fed by strong enough off-equatorial thermocline displacement, the system can end up in a permanent cold (run1b) or warm state (run1d). But the thermocline does not have a negative coupled feedback only. If the thermocline in the eastern equatorial Pacific is not allowed to adjust far enough away from

the equator via reflection into high baroclinic Rossby modes, the model ends up in a warm state (run 1f). Experiment (1e) and the many experiments (not shown) that are damped on a normal state indicate that the off-equator also plays a triggering role in the coupled oscillations. This is because it controls the low-frequency adjustment of the coupled system as explained below.

Outside the equator, the thermocline depth anomaly h (counted as positive if downwelled) is coupled to the wind stress curl anomaly as described by Equation O1:

$$\partial h/\partial t = (\beta c^2 / f^2)\, \partial h/\partial x - \text{curl}\,(\tau / \rho f) - rh \qquad \text{:Eq.O1}$$

(O1) (O2) (O3) (O4)

Term (O4) corresponds to the use of a Rayleigh friction both in the momentum equations and in the continuity equation of the baroclinic model. Checking Eq O1 at various latitudes with the results from experiment (1a), shows that local Ekman pumping (term O1=term O3) does not explain much of the variability beyond 5° of latitude. During warm events, the wind curl is weak in the western Pacific and free Rossby waves (term O1=term O2) explain part of the off-equatorial thermocline changes; actually west of the dateline, the thermocline slope flattens outs and term (O4) becomes as big as terms (O1) and (O2) because the western basin is significantly upwelled. East of 140°W, the ocean and the atmosphere are in a tightly coupled state with a strong wind curl and a steep thermocline slope. The friction term and the low-frequency changes are negligible relative to terms O2 and O3, the thermocline position tends to match the wind stress curl anomaly as in the Sverdrup equilibrium:

$$h(x) = h(East) - \int_x^{East} \frac{f}{\beta} curl\left(\frac{\tau}{\rho c^2}\right) dx \qquad \text{: Eq O2}$$

Let us analyze the balance reached by the experiments like 1bdf that are damped on a non-zero permanent state. If the final states are coupled to a zonal wind stress that has no curl, the steady-state solution to the baroclinic equations without friction verifies u=v=0 and:

$$h(x) = h(East) - \int_x^{East} \frac{\tau_x}{\rho c^2} dx \qquad : \text{Eq O3}$$

And the thermocline slopes are the same at all latitudes. This is not the case.

All the final states of experiments (1bdf) have strong wind stress curls outside the equator in the eastern Pacific, and thermoclines tilts are steep away from the equator in contrast with the gentle equatorial slopes. Results are presented for experiments 1bf in Figure 8abcd, on average over years 20 to 29 when the Niño3 SST index is slightly cold for experiment 1b and slightly warm for experiment 1f (see Fig. 6ab). The thermocline is downwelled by a few meters and almost constant all along the eastern boundary between 15°S and 15°N (dotted lines in Fig8ac), whereas it has a rough topography along the western boundary (plain lines in Fig8ac), with positions upwelled by more than 20m at 5°N and by more than 50m South of 7°S. Note that although experiment 1b ends up with a Niño3 index which is slightly negative, the final state corresponds to a downwelled thermocline in the eastern equatorial Pacific and an upwelled thermocline in the off-equatorial western Pacific. This happens because east of 120°W, the SST is positive (the Niño3 index is a misleading quantity), and the off-equatorial vortex pair in the eastern Pacific between 5° and 9° of latitude is cyclonic as during the warm events simulated by run 1a. The thermocline anomalies at the western boundary estimated with Eq O2 are oplotted in Fig. 8ac (dashed lines). For both experiments, the thermocline difference between the eastern and the western boundary is explained to a large extent by the wind stress curl, in agreement with the Sverdrup balance. There is some difference though in comparison with the Sverdrup circulation (Sverdrup, 1947) because the model has no lateral friction and currents do not verify the no-sleep condition at the boundaries, the model does not simulate intense westward return flow. Instead, the model has a Rayleigh friction, which acts as a source of mass if the thermocline is upwelled and a sink of mass if it is downwelled. The meridional transports take place in the interior of the domain without intensification at the western boundary.

For all experiments, the equatorial thermocline is much flatter than off-equator (Fig. 8bd). It verifies the balance with the zonal wind stress (Eq O3) within less than 10m discrepancy. Outside the equator, the steep slope in the eastern half of the basin matches well the balance with the strong wind stress curl (Eq O2). Differences show up in the west because of the Rayleigh term. The contribution of this term cannot be obtained by zonally integrating Eq O3. Via the continuity equation, it affects the meridional distribution of mass as well. Thus experiments (1bf) end up in a coupled state where outside the equator, the pressure difference maintained by the thermocline between the eastern and the western boundaries is much smaller than the one required by the wind stress curl and the Rayleigh term acts as a mass source in the western Pacific. Along the equator, the thermocline is slightly less tilted in the western Pacific than what is required to balance the zonal wind stress, and the Rayleigh term acts as a mass sink there. The reader should not misinterpret these results. The mismatch does not take place in the western Pacific only. In Fig8bd, the match is perfect at the eastern boundary, only because by choice Eq O3 and O2 are integrated from East to West. In the model experiments, the entire domain is involved in the continuity equation and therefore, mass adjustment is not performed in the western Pacific only. It takes place everywhere where the thermocline position is not normal. Similar structure is found for experiment 1d.

Now let us examine the processes simulated when the model oscillates as in experiment 1a. Because the system is no longer at equilibrium, results are presented for different phases of events.To cover one complete cycle, a 48-month long period simulated in experiment (1a) is chosen with the time origin at the warm peak of the Niño3 SST index. It has a positive index between months -12 and +12 corresponding to a warm event followed by fluctuations around 0 between month +12 and +36 with 3 "cold events" or "pulses" that last no longer than 6 months each (see Fig. 3a). Anomalies are averaged over 6 consecutive months and presented for phase 1 centered at the peak of the warm phase (month 0), phase 2 at the transition from warm to the first cold pulse (month 9), phase 3 at

the first cold pulse (month 15) and phase 4 at the third one (month 32). Because the system is not in equilibrium, it is not expected that the off-equatorial balance with the wind curl be respected, but this quantity is nevertheless computed as a useful reference. Balance with the zonal wind stress along the equator is also shown. It should be better verified as adjustments along the equator are faster than off-equator.

During phase 1, the thermocline is downwelled in the East and upwelled in the West as expected (Fig. 8e). This pressure gradient is well explained along the equator by the zonal wind stress anomaly (Fig. 8f). Actually, the slope along the equator is slightly steeper than what is required to balance the zonal wind stress derived from (Eq.O3). Along the western boundary, the thermocline is the shallowest at 5°S and 5°N, where it matches well the position derived from (Eq. O2) to balance the wind stress curl, but poleward of this latitude it is far from being shallow enough. Results are presented along 9°S in Fig. 8fhjl to illustrate how the South compares to the equator. Along 9°S the thermocline slope is much less steep than what is needed to balance the strong wind stress curl (Fig. 8f). One can expect that the coupled system will evolve by rising up more its thermocline in the western Pacific, even when the curl starts weakening.

During phase 2, the thermocline is not downwelled anymore along the eastern boundary, except for latitudes higher than 10°. However, it is shallower than in phase 1 along the western boundary for all latitudes, especially between 5° and 11° (Fig. 8g). The wind curl anomalies at 9° of latitudes that were huge 9 months ago have significantly decreased, but they are still strong South of 5°S. The equatorial thermocline (Fig. 8h) is now upwelled all along the basin. The thermocline along 9°S is then in much better position to balance the wind-stress curl. Note that to better verify the balance with the wind, the thermocline in the West should be upwelled more along 9°S by about 15 m and less along the equator by a similar amount.

During phase 3, the thermocline is shallow all along the eastern boundary (Fig. 8i). At the western boundary, it is close to normal in the equatorial band, but significantly

upwelled outside. The strongest wind curl is located in the North but it does not affect much the thermocline there because it does not last long (see next Fig.). The equatorial slope is tilted with the thermocline shallower in the east than in the west as expected during a cold event (Fig. 8j). But the thermocline is upwelled almost everywhere along the equator as well as for the whole basin along 9°S. At that latitude, its pattern ressembles the one 6 months ago, consistently with the fact that the ocean has a long memory and that the wind curl was already balanced then.

A period as long as 18 months with 3 cold pulses is necessary after phase 3 to recover from this basin-wide upwelled ocean. During phase 4, the thermocline is normal or slightly deep for almost all latitudes both on the eastern and western boundaries (Fig. 8k). The equatorial thermocline is downwelled for all longitudes with the deepest positions on both sides (this does not correspond to expectations for a cold event). Note that the western Pacific is slightly deeper than required by the equatorial zonal wind stress (Fig. 8l). The deepest thermocline in Fig. 8l is in the western off-equatorial Pacific. Indeed Fig8k indicates that the reservoir of warm waters accumulated prior to the growth of a warm event is in the South Pacific and not in the North. Only after this phase can a warm event grow again (the model will reach its following warm peak 15 months after).

To conclude this section, the results presented above correspond to the four phases described in the "ocean recharge paradigm" (Jin , 1997a, Fig. 1) with some refinements due to the fact that the CZ simulations are not refered to a zero mean nor filtered in time as in the latter reference. For CZ, a warm event lasts about 18 months, i.e. 3 times more than a cold event. Anomalies at the warm peak are about 3 times larger than at a cold peak. Note that in order to highlight the preconditioning of a warm event during the transition between the cold and warm phases, phase 4 in Fig. 8 has been centered at a cold peak. If it had been centered at the transition when the Niño3 SST index is zero as in Jin (1997a), the average would have been biased towards the warm conditions that have a bigger amplitude. For both papers, the thermocline along the equator is upwelled everywhere during the

transition from warm to cold (phase 2), and downwelled everywhere during phase 4. However, a striking and unexpected feature reproduced by CZ is the shallow thermocline in the southwestern Pacific during the cold phase (phase 3) and the fact that the ocean is upwelled during 40 months out of 48 all over the basin. Besides, an important aspect specific to CZ is that the off-equatorial curl is actually more energetic than the equatorial wind, with an east-west thermocline difference of more than 150m in order to balance it, compared to 50m along the equator. Another particularity is the asymmetry with respect to the equator and the dominant role of the South for preconditioning the growth of warm events. Let us examine how the anomalies propagate zonally and meridionally with time.

c) Spatio-temporal evolution of the coupled anomalies

The spatio-temporal evolution of the oscillation is illustrated in the Hovmoeller diagrams presented in Figure 9. The first 24 months that correspond to the warm events are very different from the rest of the time when the coupled system varies frequently with fast and extended zonal displacements that have a relatively confined meridional extension away from the equator. By contrast during warm events, changes in time are slow, anomalies stay pretty stable in space, with strong thermocline tilts maintained over a relatively narrow zonal front that migrates very slowly and that are extended far away from the equator.

During warm events, a thermocline front of about 1 meter per 100 km is maintained in the central Pacific where the westerlies are the strongest (Fig. 9de). Note that in reality or in forced experiments, it is very unusual to find steep anomalous fronts along the equator that stay for more than a year confined in the middle of the equatorial Pacific. Similar fronts are also found off-equator (Fig. 9abgh). In the central-eastern basin, coupled adjustements are propagating in time and space very slowly compared to free Kelvin and Rossby waves. Along the equator adjusment is done at 4 cm/s to the east for the thermocline (Fig. 9d), while wind (Fig. 9e) and SST (Fig. 9f) are standing modes. In the eastern off-equatorial Pacific, the off-equatorial curls are so strong there that they can

even drag the thermocline eastward (Fig. 9ag). Along 9°N a huge curl coupled to the SST appears 1 month after the warm peak (Fig. 9bc). It drives the thermocline at about 40cm/s to the East during the following 3 months (Fig. 9a). Along 9°S the curl (Fig. 9h) drives the thermocline slowly to the East during 6 months prior to the warm peak (Fig. 9g). White et al (1997) demonstrate why the coupling of the ocean with the wind curl in the tropics slows down the westward propagation of the free Rossby waves. The coupling simulated by CZ is so tight in the eastern Pacific that it can even reverse the free tendency.

The anomalies are not symmetric with respect to the equator. The SST is very strong and positive far South whereas it is very weak North of 3°N (Fig. 9l). The coastal SST signal south of the equator starts warming ten months prior to the warm peak because it feels the impact of the baroclinic anomalies (terms T3 and T6) in the growing warm phase. The curl anomaly in the North is stronger than in the South but it does not last as long and is more confined in latitude (Fig. 9k). The curl in the North involves nonlinearities with the climatological winds as explained in Section 6c. The important aspect here is that its evolution is not as much coupled to the slow oceanic adjustments as in the South. Because the curl in the South lasts much longer and is well established over a wide region, the thermocline gets more upwelled in the South (Fig. 9agj). The curl starts growing prior to the warm event with the coastal SST maximum. Averaged over the whole Pacific, the equatorial oceanic heat content reverses at the warm peak. The off-equatorial ocean started loosing heat content 6 months before and will continue loosing it to reach a minimum 9 months after (Fig. 9j). Poleward propagation is then found in the ocean, wind and SST signals.

The coupling system works very differently during interevents (month 12 to 36). SST minima are located South of the equator (3°S) in the central Pacific, not in the East (Fig. 9l). The associated off-equatorial curls are much weaker all over the basin, particularly in the eastern part. There is no SST minimum along the coast (Fig. 9cfi). Thermocline, SST and wind anomalies all propagate westward. In the equatorial band, the

anomalies of thermocline, SST and wind components propagate fast (90cm/s) all across the basin (Fig. 9cdefi). The propagation is westward even along the equator, because the SST changes are then dominated by term T1 of the SST equation (see Fig. 7), i.e. by the anomalous baroclinic zonal current anomalies which amplitude at the equator is stronger for the first Rossby mode than for the Kelvin mode. Thus the equatorial ocean never varies as free Kelvin waves. It does not vary either as wind forced displacements accordingly to the slow eastward mode proposed by Chao and Philander (1993) that is reasonably well reproduced by the "control run" (see DP96). The coupled ocean-SST-easterlies in the equatorial band all propagate westward. The off-equatorial curl anomalies propagate similarly fast to the west (Fig 9bh). The thermocline then propagates at a speed similar to free Rossby waves (Fig. 9ag). Note the asymmetry relative to the equator. The SST anomalies are stronger in the South than in the North (Fig. 9cil). The curl in the North is not as homogeneous as in the South, changes are fast (Fig 9bk) and the thermocline is rather influenced by reflection at the eastern boundary and by the continuity equation (Fig 9a). The basin-averaged thermocline continues recovering from the past warm event and gets downwelled in the South during the second cold pulse about 18 months prior to the next warm peak (Fig. 9j). It propagates from the South towards the equator (Fig. 9j). Using the velocity output of run 1a, it was verified that this corresponds to an interior mass transport mostly pronounced over the central Pacific between 120°W and the dateline. The equatorward propagation is also seen in the curl and the SST in the eastern Pacific. Consistently with Wyrtki (1985), Cane and Zebiak (1985) and Jin (1997ab), the equatorial ocean gets recharged with heat content before a warm event grows.

These coupled mechanisms do not correspond at all to the ones simulated by the CZ model forced by observed winds. The latter ressemble a lot more to the observations which the reader can check in Fig.8, 16, and 20 presented in Part II. Let us examine the impact of applying the changes that improved the simulations in a forced context.

6. Impact of applying Fric, Tsub or Conv on the coupled behavior.

a) Fric

Validation with XBT and current meters recommends the use of a 6 month decay time for the Rayleigh coefficient (Perigaud and Dewitte, 1996). With such a friction, the CZ model forced by FSU winds simulates zonal current anomalies along the equator that do not fluctuate every 9 month, but reverse between cold and warm events as observed current anomalies. It also simulates thermocline displacements following events in the western Pacific with a weaker amplitude. Increasing the friction is now tested in a coupled context.

Although low sensitivity to the friction is found when the model is tested with decay times longer than 30 months (see Zebiak and Cane, 1987), it is expected to find a high sensitivity of the coupled behavior to shorter decay times because a stronger friction is certainly going to affect the off-equatorial baroclinic ocean, which is involved in the triggering and reversing of the oscillations. A priori, one could anticipate that the use of a decay time much shorter than 30 months, is going to damp the model oscillations. This is not the case at all (Fig. 10). Because there is so much energy in the off-equatorial baroclinic ocean coupled to the equatorial SST, the CZ model with a 6 month decay time reproduces strong warm events every 9 years (Fig. 10a). This experiment also exhibits the presence of the "mobile mode" on top of the low-frequency events. The warm events last longer than in run 1a. A possible interpretation is the following. The off-equatorial baroclinic anomalies coupled to the wind stress curls in the eastern Pacific are more damped when they reach the western boundary. Therefore the model needs the contribution of the baroclinic ocean further away from the equator to erode the growing warm anomalies in the eastern equatorial Pacific. As the propagation of Rossby waves is slower at higher latitudes, it takes more time for the western Pacific to reach the upwelled position necessary to erode the warm event. Indeed this experiment simulates thermocline displacements at the warm peak that are maxima along the western boundary 2° poleward of run 1a.

However increasing the friction does not only increase the dissipation of momentum but also the change rate of mass, and the role of the off-equator in recharging the system from the interior of the domain is also more efficient. So this interpretation does not always hold.

Because of nonlinearities, it is not true that the period of oscillations increases with the friction. Coupled simulations with decay times equal to 12 months (Fig10b) or 15 months (Fig10c) display very different oscillatory behaviors. The validity of the conclusions derived from 30 year-long integrations even depends on the initial conditions. This is illustrated in Fig. 10d for two simulations which both have a 20 month friction, but one is initiated in July 1988 and the other one in January 1989. In any case, increasing the friction is not going to reduce model errors as long as simulations are strongly as in CZ.

b) Tsub

Guided by DP96, the most crucial modification to apply in order to reduce this bias is the Tsub one that allows to recover cold SST and easterlies in a forced context. The Tsub parameterization is significantly different from CZ in case of thermocline upwelling. Typically for a thermocline upwelled by 20m at 140°W (90°W), the Tsub decrease is 10 (30) times larger than the one assumed in CZ. In case of downwelling, the fit to hydrographic data gives much smaller modifications. For a thermocline downwelled by 20m at 90°W, the Tsub increase is 1.2 times weaker than in CZ.

The ocean model with Tsub is now tested in a coupled experiment named Tsub.CZ (run2). It simulates two-year oscillations during the first 12 years followed by a more irregular behavior (Figure 11a). A lag as big as 6 months is now found between the zonal wind stress time series (Figure 11b) and the SST time series. Unexpectedly, Tsub.CZ does not reproduce SST anomalies colder than in the standard case (run 1a). It does not simulate easterlies either, and the bias is not reduced at all. Indeed past year 20, the model

is in a permanent anomalous state with warm SST, westerlies, deep thermocline in the East (Fig. 11c) and shallow in the West (Fig11d).

Moreover Tsub change affects the spatial patterns. Compared to CZ (run 1a), the off shore SST maximum along the equator is shifted to the West at 140°W, instead of 110°W (Fig. 12a) and the amplitude is twice larger than in reality. It sharply decreases with increasing longitude, and the coastal maximum South of the equator is not reproduced. Conversely to results in DP96, the impact of Tsub modifications on the SST is far from linear. Typically, a 1000% increase of cold Tsub has very little impact, and a 20% decrease of warm Tsub reduces the SST amplitude east of 90°W by a factor 2. This happens because nonlinearities have grown in the coupled case, so much that SST variations are not even positively correlated with the thermocline variations in the eastern Pacific. Following the approach presented in section 5, the authors analyzed the seven terms involved in the surface heat budget simulated by Tsub.CZ and found that like in CZ for term (T6) in the eastern Pacific, an upwelled thermocline does not have a cooling, but a warming impact on the SST. This feature is thus not due to the weak cooling of the subsurface assumed in CZ (run 1a). Tsub.CZ does simulate a strong Tsub cooling when the thermocline is upwelled, but term (T6) still has a warming impact on the SST, because the Tsub anomaly is still weaker than the SST anomaly. The latter is more efficiently cooled down by the local anomalous upwelling (term T5).

Even though the Tsub parameterization displaces the SST maximum to the West compared to CZ (run 1a), it does not affect much the location of the wind maximum along the equator (Fig. 12b). This is because the wind simulated by the atmospheric model is sensitive to the gradients of SST which are very similar west of 130°W to Tsub.CZ and CZ. Tsub.CZ also simulates spurious easterlies east of 80°W at the equator and in the off-equatorial eastern Pacific. Thus changing the oceanic parameterization only has not corrected the major deficiencies described in the previous sections. Deficiencies may rather be due to the atmospheric component.

c) Conv

The wind patterns simulated by CZ or Tsub.CZ are consistent with the role of SST gradients in forcing low-level winds (Lindzen and Nigam, 1987). Gill (1980)'s model, based on similar physics (Neelin, 1989) also tends to shift the wind eastward of reality, because it is forced by local heating only. In Nature, the heat is released in the atmospheric layer where the convection occurs, which is not where the SST anomalies are maximum, but closer to where the surface winds converge and rise. For this reason, the CZ atmosphere is not only driven by local heating as in Gill (term named Q_T), but also by a term which is a function of the surface wind convergence (term named Q_C). Q_C helps confine the wind patterns equatorward (see Zebiak, 1986). These terms are given by the equations (see Appendix in Zebiak and Cane, 1987) :

$$Q_T = \alpha T \exp [(\underline{T} - 30) / 16.7] \quad : \text{Eq A1}$$

$$Q_C = -\beta [M(C+\underline{C}) - M(\underline{C})] \quad : \text{Eq A2}$$

with $\alpha = 0.031$ m^2 s^{-3} °C^{-1} and $\beta = 1.6 \times 10^4$ m^2 s^{-2}. T is the sea surface temperature anomaly and C the anomalous wind convergence. Underlined variables and the M function have the same meaning as in Eq T.

In a forced context, CZ simulates equatorial westerlies slightly to the east of reality and a curl in the south-east Pacific which is stronger. These deficiencies are reduced when the model is forced with the heat anomalies released by high-cloud convection derived from ISCCP data added to the local heating derived from observed SST anomalies with α = 0.015 m^2 s^{-3} °C^{-1}. Because the observed convective heat anomalies are well approximated by :

$$Q_{CN} = \gamma \, \mathrm{Conv}(x,y) \; N3 \quad : \text{Eq A3}$$

where Conv(x,y) is the first eigenvector of the EOF decomposition of data, N3 is the Niño3 SST index and $\gamma = 1.13 \times 10^4$ m^2 s^{-2} °C, the atmospheric model forced by Eq A1 and A3 with observed SST reproduces well the observed wind stress along the equator and off-equator (see DP96). Whether the model is run in a forced or in a coupled mode,

Eq A3 warranties that Q_{CN} is located in the central and western Pacific along the ITCZ and SPCZ. By contrast, Q_C in CZ does not help drag the wind westward because it grows and is displaced to the eastern Pacific in a coupled mode. During warm events simulated by run 1a, convergence anomalies get stronger than the climatology in the eastern Pacific, the atmosphere receives the heat anomaly $Q_c = - \beta (\underline{C} + C)$ south of the ITCZ where mean winds are divergent. Q_C thus increases the off-equatorial easterlies and curl. It plays an important role in destabilizing the system (Tziperman et al, 1997). Indeed the experiment where the CZ model is run with Q_C=0 at each time step (not shown) simulates the strongest warm events and bias among all the experiments presented in this paper.

The atmospheric model with Eq A1 and A3 is now tested in a coupled experiment named CZ.Conv (run3). It gives oscillations every 4 years (discussed further below), but the important result examined here is that their amplitude is weak and centered around a normal state (SST anomalies stay within +/- 0.8°C). Conv has a major impact on the coupled behavior. Dragging the forcing of the atmosphere model westward reduces the coupled feedback between the warm SST and the surface wind convergence on inducing anomalous downwelling (term T5). Oscillations are then no more biased. Thus it is the coupling with the CZ atmosphere that significantly contributes to the warm bias simulated by CZ or Tsub.CZ.

The drag coefficient is then increased by 20% in an experiment named CZ.Conv (run 4). Oscillations have a much more realistic amplitude than in CZ.Conv (run 3). The period is also close to 4 years, it is slightly longer than in run 3 consistently with the sensitivity to increased drag coefficient found in CZ (see Zebiak and Cane, 1987). Both experiments exhibit similar patterns. This is quite remarkable, because changing the drag usually affects the spatial distribution of the anomalies simulated by models run in a coupled context (exemples will be given in Part II). The SST variability simulated by CZ.Conv (Fig. 13a) agrees resonably well with observations. The zonal wind stress (Fig.

13b) has a maximum along the equator which is shifted to the west compared to CZ and much closer to reality. Note however that the wind maps still present the spurious features in the off-equatorial eastern Pacific like in CZ or Tsub.CZ.

d) Intercomparison

CZ.Conv (run 4) is now compared with CZ (run 1a), Tsub.CZ (run 2) and observations. All models simulate a thermocline variability beyond 5° of latitude that is two to three times larger than in reality (Fig. 14a). They also simulate large zonal wind anomalies in the eastern Pacific that correspond to cyclonic curls beyond 5° of latitude stronger than the observed ones by a factor of 2 at least (Fig. 14b). Note that the observed variability in the eastern Pacific may be overestimated (see Part II). CZ.Conv succeeds in dragging the curl significantly to the west (maximum at 160°W) of CZ or Tsub.CZ (maxima at 130°W).

CZ.Conv is also the model that is the closest to reality for the variability of the SST and the zonal wind stress along the equator (Fig. 15). For both signals, it simulates amplitudes and patterns in good agreement with the observed ones, except for the strong increase east of 100°W in the wind. It is quite striking that Tsub.CZ has a weaker variability there, together with a significant decrease of SST amplitude towards the coast. Intercomparison of these results illustrates that this deficiency cannot be attributed more to the ocean component than to the atmospheric one, it is a nonlinear mode of growth that takes place in the coupled context only.

The sole analysis of the spatial variability can be misleading. Time series reveal that CZ.Conv (run 4) has a severe warm bias (Fig. 16). Like in CZ, interevents are dominated by a series of fluctuations similar to the "mobile mode" with 3 weak and brief cold events. Warm events last long and have much stronger anomalies, the thermocline in the western Pacific shows particularly strong displacements. Indeed the 30 year averaged thermocline is also upwelled by 20m. Part of this warm bias is due to the nonlinearity of the negative feedback term (T6) with the climatological upwelling rate in the Central-

Western Pacific: as explained in section 5a, upwelled thermocline does not contribute as much to cool down the SST as a downwelled thermocline warms it up. Part of it is due to the nonlinearity of the positive feedback term (T5) that dominates the SST variations in the eastern Pacific: an upwelled thermocline in the eastern Pacific does not contribute to cool but warm the system. As explained in Xue et al (1997), Tsub and the advection terms of SST are important forms of nonlinearity. In a forced context, the only noticeable nonlinearity is the Tsub one. T5 and T6 are the non linear terms that happen to grow in a coupled context for all the models presented in this paper. Nevertheless time series simulated by CZ.Conv also show that the Niño4 wind index varies simultaneously with the SST index without lag. This is another important improvement of CZ.Conv compared to the other models.

7. Summary of results and Consequences

One lesson learnt in this study is that results drawn from coupled simulations should never be generalized. Nonlinearities can grow in a coupled context, leading to mechanisms that can be far from those involved in a forced context. Coupled ocean atmosphere models which are based on similar physics can lead to opposite conclusions depending on details that have a negligble impact on forced simulations. For instance, the CZ model needs the off-equatorial variability in order to sustain ENSO-like oscillations whereas the Battisti (1988) model does not. The CZ model does not work as a "delayed oscillator".

It drastically depends on the off-equatorial signals to trigger warm events as well as to reverse growing warm anomalies. The equatorial SST is coupled to the off-equatorial wind stress curl. This one does not induce thermocline displacements via Ekman pumping, but is rather coupled to the ocean via quasi-Sverdrup equilibrium. High Rossby modes are responsible for diffusing heat content away from the equator on the eastern side and eroding warm events from the interior and the western side. It also recharges the equatorial

heat content prior to a warm event. It is this low-frequency adjustment involving the whole domain that allows the third cold pulse to kick off the following warm event. On one hand, these results are consistent with the idea of the recharging of the equatorial "reservoir of warm water" as a necessary precondition for the initiation of a warm event (Wyrtki, 1975; Wyrtki, 1985; Cane and Zebiak, 1985; Cane, 1992a) and with the "recharge oscillator paradigm" proposed by Jin (1997ab). On the other hand, they highlight some characteristics of the CZ model that are not described elsewhere. The east-west thermocline depth difference balancing the wind anomalies induced per 1°C of SST anomaly is three times bigger at 9° of latitude than at the equator, the whole ocean is upwelled 40 months out of 48, cold events are not the converse of warm events, the South is more tightly coupled because of the cold tongue than the North which undergoes irregular variations associated with the ITCZ and the equator is recharged by the South.

The CZ model drives westerlies along the equator that require more gentle thermocline slopes compared to the pressure necessary to balance the associated curl anomalies beyond 5° of latitude in the eastern Pacific. This becomes a major problem only when the model components are coupled. The role of off-equatorial winds and ocean variability on ENSO behavior has been a subject of controversy for long (see e.g. McCreary and Anderson, 1991; Graham and White, 1991; Kessler, 1991; Wakata and Sarachick, 1991). More and more evidence of the role of the off-equatorial signals in ENSO can be found in the litterature (White et al, 1997; Zhang and Levitus, 1997). The authors are convinced that this role should no longer be neglected. A very important goal to reach is to reduce errors in the off-equator and reproduce wind and thermocline anomalies in the ITCZ and SPCZ that at least have the correct sign. Although forced experiments with Fric, Tsub and Conv perform reasonably well on this aspect, it is not certain at all that ICMS can do so in a coupled context. In any case, the lesson learnt here is that thorough validation and analysis of the coupled results are necessary outside the equatorial band as well as inside.

The need for examining model outputs beyond indices is also pointed out. We gave several examples of coupled simulations where the Niño3 SST index oscillates with a period close to 4 years with some irregularity, but are far from reproducing realistic ENSO. Box-averaged indices elsewhere than in the eastern Pacific are necessary, including fields like the wind or the thermocline. In addition to the oscillation period, it is useful to check if time series are biased or not. Amplitudes and spatial patterns are important aspects to consider as well. Horizontal and vertical current anomalies must not be ignored either. Because these fields are more difficult to validate by direct comparison with observations, analyzing the heat budgets provide some useful insight and allows to find out the growing nonlinearities of the coupled system.

Limitations in the model's ability to simulate the real system and sensitivities of its coupled behavior have been addressed in Zebiak and Cane (1987). There is nothing fundamentally wrong about the basic physics assumed in the CZ model, neither in the ocean nor in the atmosphere. Even though it is only when coupled that simulations become very unrealistic, the coupling itself is not unreasonable either. The concept of heat exchange via term T7 in Eq T and Q_T in Eq A1 only, is certainly simplified compared to the actual momentum, heat and water exchanges at the air-sea interface, but it works to some extent in representing the observed heat loss of the ocean to the atmosphere during a warm event (Weare, 1983). Rather than adding more physics to the model, it is worth first to use the data that became available since the model was designed to improve the parameterizations and test their impact on the coupled behavior.

One of the most striking feature of the coupled system simulated by CZ, is a bias towards anomalous states with warm SST in the East, strong westerlies in the Central, and large upwellings of thermocline in the West, while cold events are brief and mild. A priori this could have been due to the parameterization of the subsurface temperature which assumes a very little change in case of thermocline upwelling. However changing the sole Tsub parametrization does not reduce this deficiency, as it does in the forced

experiment..The wind is located 30° to the East of the dateline, in a region where the change of upwelling rate due to locally induced Ekman currents overpowers the role of the thermocline so badly, that either the thermocline displacements have a minor impact (in case of downwelled thermocline) or compete the SST trend (in case of upwelled thermocline).

Deficiencies are reduced by replacing the CZ atmosphere component by Conv. Without the moisture convergence feedback, the lag between the SST and the wind is suppressed. CZ.Conv simulates a zonal wind stress maximum along the equator which is located about 30° westward of the position given by CZ or Tsub.CZ. This is a lot closer to reality. But CZ.Conv reproduces oscillations that are too weak and with a stronger drag coefficient, it also misses cold events and is biased again towards an anomalous state with quasi-permanently upwelled thermocline in the West. In any case, one should remember that the impact of a change in one component of the coupled system is very different whether it is tested in a forced or in a coupled context because of the growth of nonlinearities in the latter. Tsub.Conv is still a nonlinear model. So one cannot predict the coupled behavior of Tsub.Conv without testing, analyzing and validating it, as proposed in Part II.

Acknowledgments

The authors at the Jet Propulsion Laboratory, California Institute of Technology were supported under contract with the National Aeronautics and Space Administration. They thank Drs S. Zebiak and M. Cane from Lamont Doherty Earth Observatory for providing their code of the coupled ocean-atmosphere model, input files, initialization procedure as well as their time and helpful discussions.

Bibliography

Battisti, D. S., 1988: Dynamics and thermodynamics of a warming event in a coupled tropical atmosphere-ocean model. *J. Atmos. Sci.*, **45**, 2889-2819.

Battisti D.S., 1989: "On the role of Off-equatorial Waves during ENSO", *J. Phys. Oceanog.*, **19**, 551-559.

Boulanger, J.-P. and L.L. Fu, 1996: Evidence of boundary reflection of Kelvin and first-mode Rossby waves from TOPEX/POSEIDON sea level data, *J. Geophys. Res.*, **101**, 16,361-16,371.

Cane M.A., 1992: Tropical Pacific ENSO models: ENSO as a model of the coupled system. *Climate System Modeling*, K. Trenberth Ed., Cambridge University Press, 583-616.

Cane, M. A., and S. E. Zebiak, 1985: A theory for El Niño and the Southern Oscillation, *Science*, 228, 1084-1087.

Cane, M. A., S. E. Zebiak, and S.C.Dolan, 1986: Experimental forecasts of El Niño, *Nature*, **321**, 827-832.

Chao, Y. and G. S. Philander, 1993: On the structure of the Southern Oscillation. *J. Climate*, Vol **6**, n°3, 450-469.

Climate Diagnostics Bull., Near real-time analyses Ocean/Atmosphere, Climate Prediction Center, US department of Commerce, National Oceanic and Atmospheric Administration, National Weather Service W/NP52, Room 605, Stop9910, Washington DC 20233-9910.

Deser C., and J.M. Wallace, 1990: Large scale atmospheric Circulation Features of warm and cold episodes in the tropical Pacific, *J. Climate*, **3**, 1254-1281.

Dewitte B. and C. Périgaud, 1996: El Niño-La Niña events simulated with Cane and Zebiak's model and observed with satellite and in situ data. Part 2: model forced by data., *J. Climate.*, 9, 1188-1207.

Gill, A. E., 1980: Some simple solutions for heat induced tropical circulation. *Q. J. R. Meteor. Soc.*, **106**, 447-462.

Goldenberg, S. B. and J.J. O'Brien, 1981: Time and space variability of tropical Pacific wind stress. *Mon. Wea. Rev.*, **109**, 1190-1207.

Graham N.E. and W. B. White, 1991: Comments on "On the role of off-equatorial oceanic Rossby waves during ENSO", *J. Phys. Oceanogr*, **21**, 453-460.

Jin F.F., 1997: An equatorial Ocean Recharge Paradigm for ENSO. Part I: Conceptual Model, *J.Atmos. Sc.*, **54**, 811-829.

Jin F.F., 1997: An equatorial Ocean Recharge Paradigm for ENSO. Part II: A Stripped-Down Coupled Model, *J.Atmos. Sc.*, **54**, 830-847.

Kessler, W. S., 1991: Can reflected extra-equatorial Rossby waves drive ENSO? *J. Phys. Oceanogr.*, **21**, 444-452.

Kirtman B.P., 1997: Oceanic Rossby wave Dynamics and the ENSO period in a coupled model, *J. Climate*,

Kleeman R., 1993: On the dependence of hindcast skill on ocean thermodynamics in a coupled ocean-atmosphere model. *J. Climate*, **6**, 2012-2033.

Lindzen, R.S. and S. Nigam, 1987: On the role of sea surface temperature gradients in forcing the low-level winds and convergence in the tropics. *J. Atmos. Sci.*, 45, 2440-2458.

Mantua N.J. and D.S.Battisti, 1994: Evidence for the delayed oscillator mechanism for ENSO: the "observed" Oceanic Kelvin mode in the far western Pacific. *J. Phys. Oceanog.*, **24**, 691-699.

Mantua N. J. and D. S. Battisti, 1995: Aperiodic variability in the Cane-Zebiak coupled ocan-atmosphere model: Ocean-atmosphere interactions in the western equatorial Pacific. *J. Climate*, **8**, 2897-2927.

McCreary, J.P., and D.L.T. Anderson, 1991: An overview of coupled ocean-atmosphere models of El Niño and the Southern Oscillation, *J.Geophys. Res.*, **96**, 3125-3150.

Neelin, J. D., 1989: On the interpretation of the Gill model. *J. Atmos. Sc.*, **46**, 2466-2468.

Neelin, J. D., 1991: The slow sea surface temperature mode and the fast-wave limit: Analytic theory for tropical interannual oscillations and experiments in a hybrid coupled model. *J. Atmos. Sci.*, **48**, 584-606.

Périgaud, C., and B. Dewitte, 1996: El Niño-La Niña events simulated with Cane and Zebiak's model and observed with satellite and in situ data. Part 1: model data comparison., *J. Climate.*, **9**,1,66-84.

Perigaud C, S. Zebiak, F. Melin, JP Boulanger and B. Dewitte, 1997: On the role of the meridional wind anomalies in a simple model of ENSO, *J. Climate.***10,** 761-773.

Reynolds, R. W. and T.M. Smith, 1994: Improved global sea surface temperature analyses using optimal interpolation, *J. Climate,* **7**, 929-948.

Schopf P.S. and M.J. Suarez, 1988: Vacillations in a coupled ocean-atmosphere system, *J.Atmos. Sci.* , **45**, 3283-3287.

Smith N.R., J.E. Blomley and G. Meyers, 1995: An improved system for tropical ocean sub-surface temperature analyses, *J. Atmos. Oceanic. Technol.*, 219-256.

Sverdrup H.U., 1947: Wind-driven currents in a baroclinic ocean. *Proc. Nat. Acad. Sci.*, **33**, 318-326.

Tziperman E., S.E. Zebiak, and M.A. Cane, 1997: Mechanisms of seasonal-ENSO interaction", J. Atmos. Sci., **54**, 61-71.

Wakata Y.and E.S. Sarachick, 1991: Unstable coupled atmosphere-ocean modes in the ENSO cycle. *J. Phys. Oceanogr.*, **21**, 434-443.

Weare B.C., 1983: Interannual variation in net heating at the surface of the tropical Pacific Ocean. *J. Phys. Oceanogr.*, **13**, 873-885.

Weisberg R.H. and C. Wang, 1997: A western Pacific oscillator paradigm for the El Nino-Southern Oscillation, *Geophys. Res. Lett.*, **24**, 779-782.

White W.B., Y. He and S. E. Pazan, 1989: Off-equatorial westward propagating waves in the tropical Pacific during the 1982-83 and the 1986-87 ENSO events, *J. Phys. Oceanogr.*, **19**, 1397-1406.

White W.B., Y. Chao and C.K. Tai, 1997: Coupling of Oceanic Rossby waves with the Atmosphere in the Pacific Basin, *J. Phys. Oceanog.*

Wyrtki K., 1975: El Niño - The dynamic response of the equatorial Pacific Ocean to atmospheric forcing. *J. Phys. Oceanogr.*, **5**, 572-584.

Wyrtki K., 1985: Water displacements in the Pacific and the genesis of El Nino cycles, *J. Geophys. Res.*, **90**, 7129-7132.

Xue Y., M.A. Cane, and S.E. Zebiak: "Predictability of a Coupled Model of ENSO Using Sigular Vector Analysis. Part I: Optimal Growth in Seasonal Background and ENSO Cycles", Mon. Wea. Rev., **125**, 2043-2056.

Zebiak, S. E., 1986: "Atmospheric Convergence feedback in a simple model for El Nino", *Mon. Wea. Rev.*, **114**, 1263-1271.

Zebiak, S. E., and M. A. Cane, 1987: A model El Niño-Southern Oscillation. *Mon. Wea. Rev.*, **115**, 2262-2278.

Zhang R.H. and S. Levitus, 1997: Interannual variability of the coupled tropical Pacific ocean-atmosphere system associated with the El Nino/Southern Oscillation, *J. Climate*, **10**, 1312-1330.

Table 1: Run Identification

All simulations are identified by a name specifying the model used and a number describing the experiment. The friction and drag coefficients are the ones used in CZ, i.e. the friction decay time is (30 month), the drag is (2.00×10^{-3}) in the forced context (run0*) and (3.29×10^{-3}) in all the coupled simulations, unless specified.

Tests are done on the baroclinic model component (BAR), or the Mixed Layer Ocean component (MLO) or the Atmospheric component (ATM).

Name	Number	Description
CZ	(1a):	Standard coupled run.
CZ	(1b) :	(TX,TY)=0 beyond 9°N/S before time-stepping BAR and MLO.
CZ	(1c) :	(TX,TY) =0 beyond 9°N/S only before time-stepping MLO.
CZ	(1d):	(TX,TY)= 0 beyond 9°N/S only before time-stepping BAR.
CZ	(1e):	Only Rossby modes graver than 5 reflect into Kelvin in BAR.
CZ	(1f):	Kelvin reflects only in the 5 gravest Rossby modes in BAR.
CZ	(0a):	Standard "Control Run" forced by observed FSU.
CZ	(0b):	"Control Run" with (TX,TY) =0 beyond 9°N / S as in (1b).
CZ	(0c):	"Control Run" with only the 5 gravest Rossby modes in BAR.
Tsub.CZ	(2):	Tsub from DP96 in MLO.
CZ.Conv	(3):	Conv from DP96 in ATM
CZ.Conv	(4):	as CZ.Conv (3) with the drag coefficient multiplied by 1.2

Figure Caption

Figure 1: Time series of observed SST anomalies averaged over Niño3 (a), zonal wind stress anomalies averaged over Niño4 (b), and thermocline depth anomalies averaged over Niño3 (c) or over NiñoW (d). Plots **(a)** are derived from CAC (plain) or Reynolds data (dotted). Plots **(b)** are derived from the "detrended" (plain) and the "non-detrended" (dotted) FSU data. Plots **(cd)** are derived from the ocean heat content in the upper 400m (T400, plain) or from the depth of the 20°C isotherm (D20, dotted). Signs are positive for warm SST, eastward wind and downwelled thermocline anomalies.

Figure 2: Maps of RMS variability for the SST anomalies in Kelvin derived from CAC data **(a)** or from Reynolds data **(b)**, for the zonal and meridional wind stress anomalies in Dyn/cm^2 derived from FSU detrended data **(cd)** and for the thermocline depth anomalies in meter derived from T400 **(e).** Variability is computed over the whole duration of the data set.

Figure 3: Time series of SST Niño3 anomalies (a), TX Niño4 anomalies (b) and H anomalies over Niño3 (c) or NiñoW (d) simulated by the 30 year long coupled runs of the CZ model (run1a). To be compared with Figure 1.

Figure 4: RMS variability for the SST anomalies in Degree Kelvin **(a)**, for the zonal and meridional wind stress anomalies in Dyn/cm2 **(bc),** and for the thermocline depth anomalies in meter **(d)** simulated by CZ (run 1a). Variability is computed over the 30 years of the coupled experiment. To be compared with Figure 2.

Figure 5: Anomaly maps of thermocline depth **(ab)** or wind stress curl **(cd)**. Anomalies are averaged over 5 months after the warm peak for the thermocline, or centered around it for the curl. **(ac)** is derived from CZ (run 1a), **(bd)** from observations for the 1983 warm event. Units are meters for thermocline and 10^{-8} Pa/m for curl.

Figure 6: Time series of SST Niño3 index simulated by 30 year long coupled runs with the CZ model. **(a)** corresponds to experiments testing the role of the off-equatorial wind,

(b) to testing the role of the western or eastern boundary, **(c)** to the runs forced by FSU winds. See Table1 for run identification.

Figure 7: Rate of SST changes in °/month simulated by run 1a averaged along the equator in the western Pacific (160°E-160°W), central Pacific (160°W-120°W) and eastern Pacific (120°W-80°W) as a function of time in years. Thick line corresponds to local changes + damping (term T7). Thin line corresponds to anomalous upwelling (term T5), dotted line to thermocline displacements (term T6), dashed line to horizontal advection (terms T1+T2+T3+T4). Numbers correspond to the terms in the T Equation (see text).

Figure 8: Thermocline anomalies compared to the zonal integrations of wind anomalies given by Eq. O2 or Eq. O3. Plots correspond to the anomalies simulated by experiments 1b (**ab**), 1f (**cd**) and 1a (**efghijkl**). Left plots (**acegik**) are anomalies as a function of latitude along the eastern (EB) or the western (WB) boundary. Right plots (**bdfhjl**) are anomalies as a function of longitude. Plots correspond to averages over years 20 to 29 for experiments 1bf or over 6 months for experiment 1a which are presented during phase 1 centered at the warm peak (**ef**), phase 2 at peak + 9 months (**gh**), phase 3 at peak + 15 months (**ij**) and phase 4 at peak + 32 months (or -15 months) (**kl**).

Figure 9: Hovmoeller diagrams of the composite anomalies simulated by CZ (run 1a). Anomalies are thermocline depth in meters, wind stress curl in 10^{-8} Pa/m, SST in Degree Kelvin, and zonal wind stress in Dyn/cm^2. Straight lines in a) and g) indicate the direction of propagation of theoretical free Rossby waves .Diagrams are as a function of longitude along 9°N (**abc**), along the equator (**def**), along 9°S (**ghi**), or as a function of latitude averaged over 130°E-80°W for (**j**) over 80°W-120°W for (**k**) and along 80°W for (**l**). Vertical axis corresponds to the time in month, where month zero is centered at the warm peak of the Niño3 SST index.

Figure 10: Time series of SST Niño3 anomalies simulated by CZ model with the standard parameterization, except for the dynamic friction. The decay time of the Rayleigh friction is

given in month on top of each panel. The two plots in **(d)** correspond to two different initial conditions (January 1989 and July 1988).

Figure 11: Same as Figure 3 for Tsub.CZ (run2).

Figure 12: Same as Fig. 4ab for Tsub.CZ (run 2).

Figure 13: Same as Figure 12 for CZ.Conv (run 4).

Figure 14: RMS variability of thermocline anomalies as a function of latitude along the dateline **(a)** and of wind stress curl anomalies as a function of longitude along 9°N **(b)**. Variability is computed over 15 years of the thermocline anomalies observed with T400, 27 years of FSU wind stress, or over the 30 years of coupled runs for CZ (run1a), Tsub.CZ (run2), CZ.Conv (4).

Figure 15: Same as Figure 14 for the RMS variability of the SST **(a)** or the zonal wind stress **(b)** anomalies as a function of longitude along the equator.

Figure 16: Same as Figure 11 for CZ.Conv (run3 and 4).

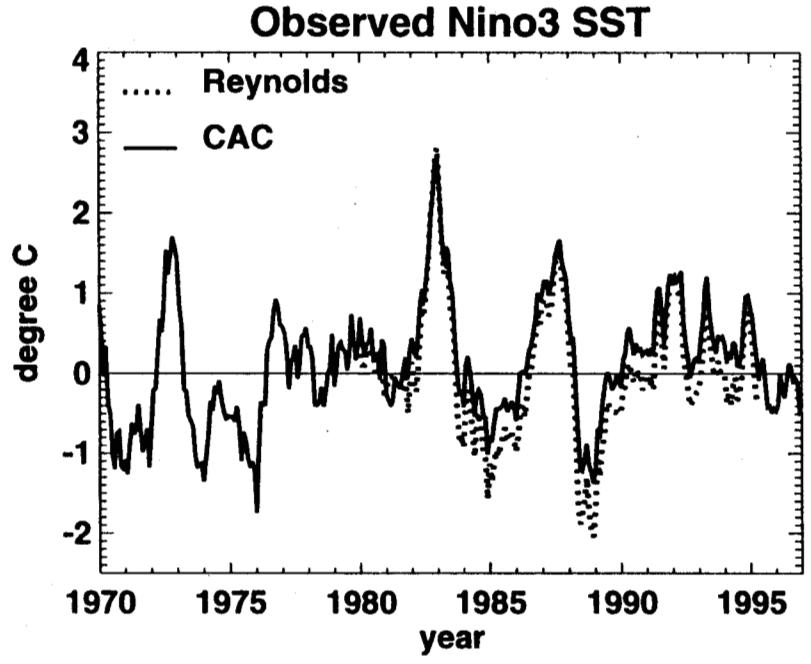
Observed Nino3 SST
Reynolds
CAC
degree C
4
3
2
1
0
-1
-2
1970
1975
1980
1985
1990
1995
year

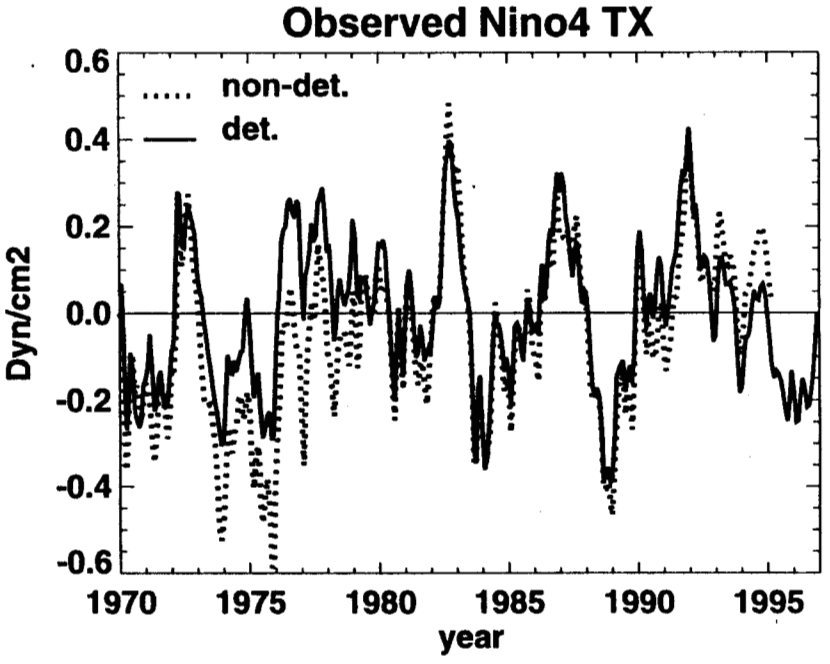
Observed Nino4 TX
non-det.
det.
Dyn/cm2
0.6
0.4
0.2
0.0
-0.2
-0.4
-0.6
1970
1975
1980
1985
1990
1995
year

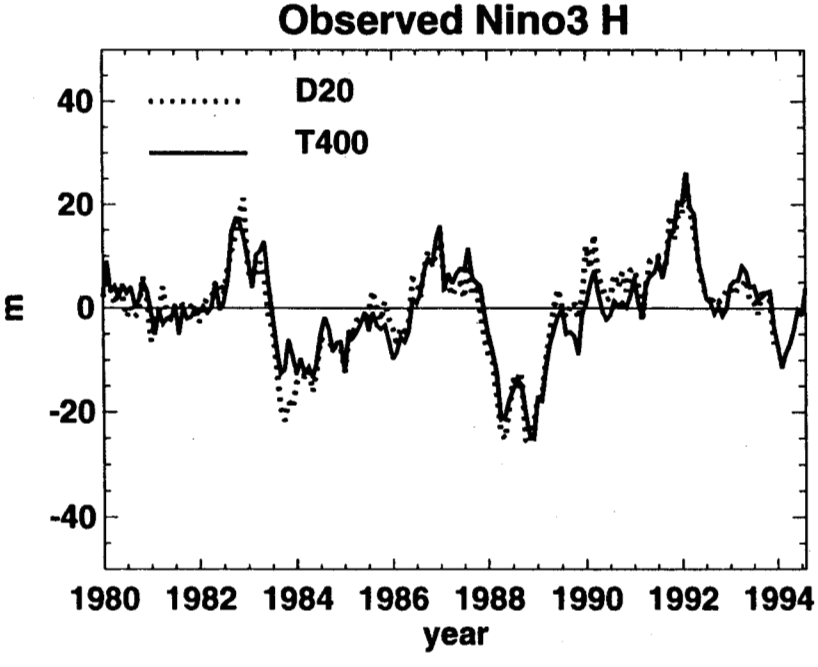
Observed Nino3 H
D20
T400
m
40
20
0
-20
-40
1980
1982
1984
1986
1988
1990
1992
1994
year

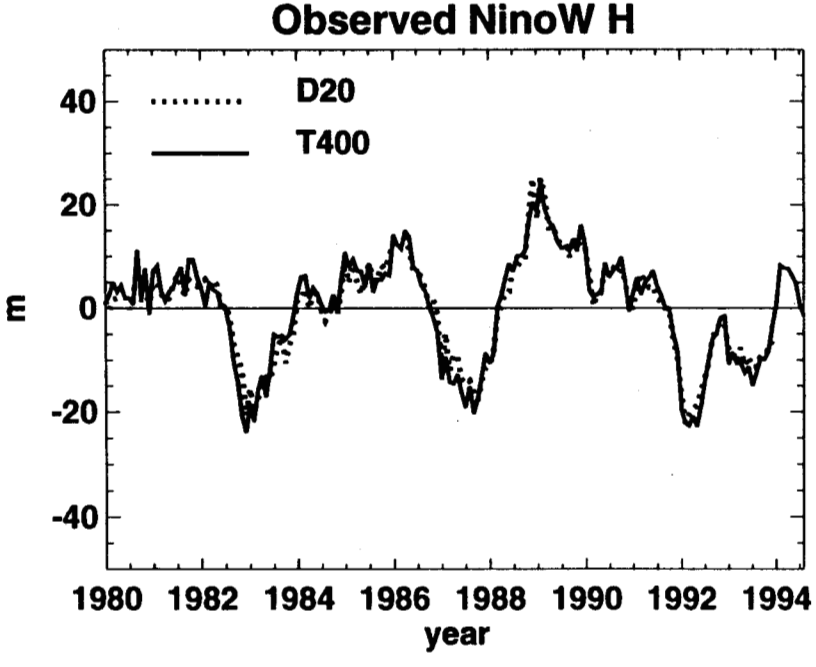
Observed NinoW H
D20
T400
m
40
20
0
-20
-40
1980
1982
1984
1986
1988
1990
1992
1994
year

Fig1.

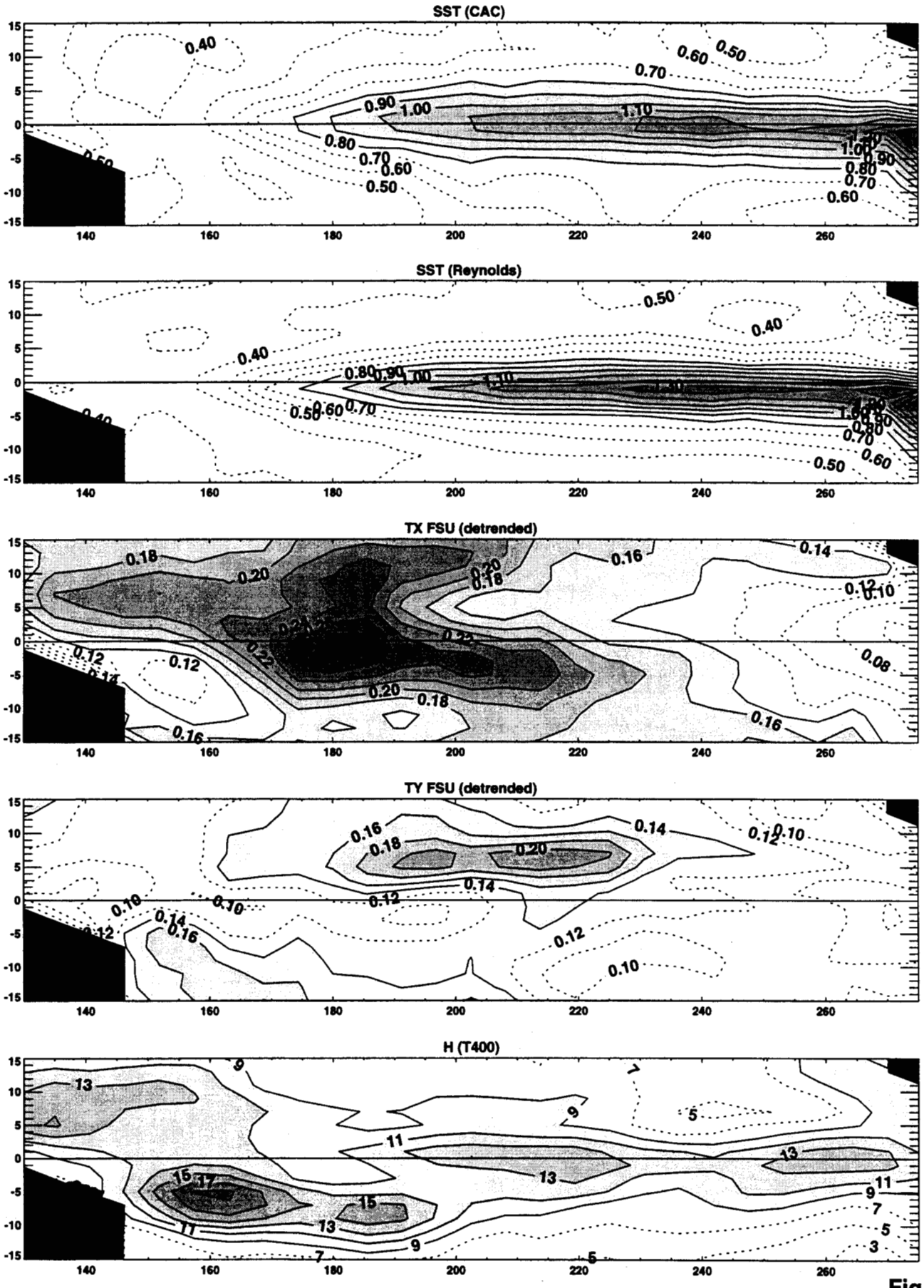
SST (CAC)
SST (Reynolds)
TX FSU (detrended)
TY FSU (detrended)
H (T400)

Fig.2

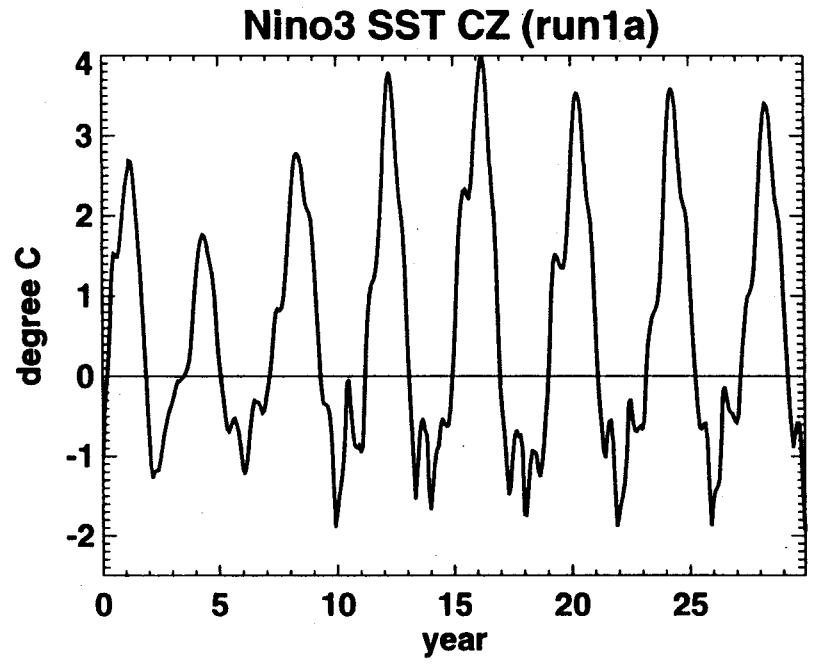
Nino3 SST CZ (run1a)
degree C
4
3
2
1
0
-1
-2
0
5
10
15
20
25
year

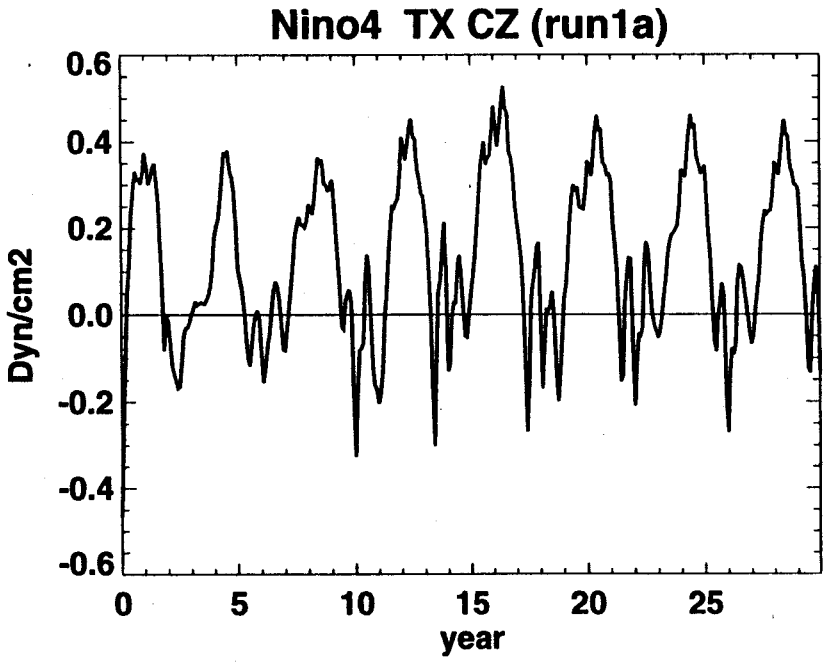
Nino4 TX CZ (run1a)
Dyn/cm2
0.6
0.4
0.2
0.0
-0.2
-0.4
-0.6
0
5
10
15
20
25
year

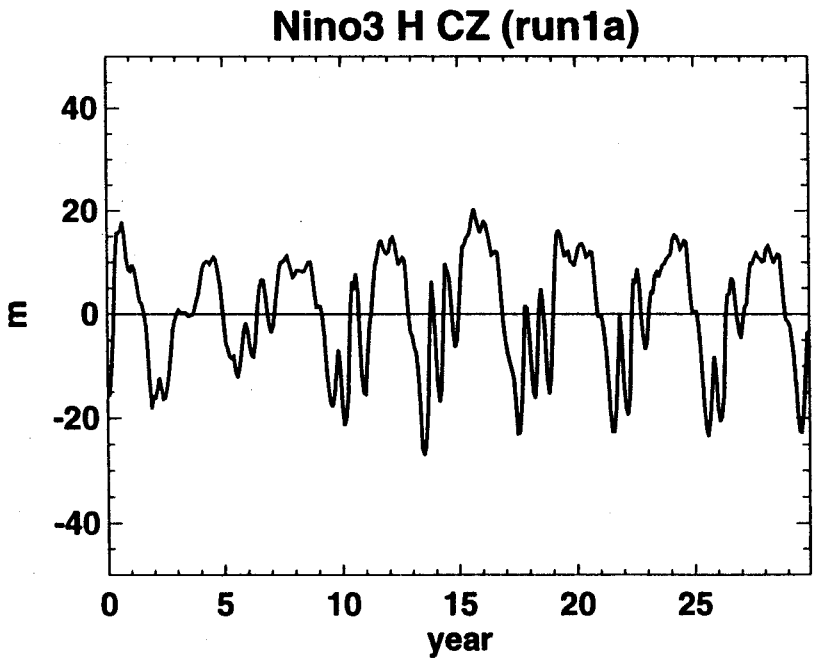
Nino3 H CZ (run1a)
m
40
20
0
-20
-40
0
5
10
15
20
25
year

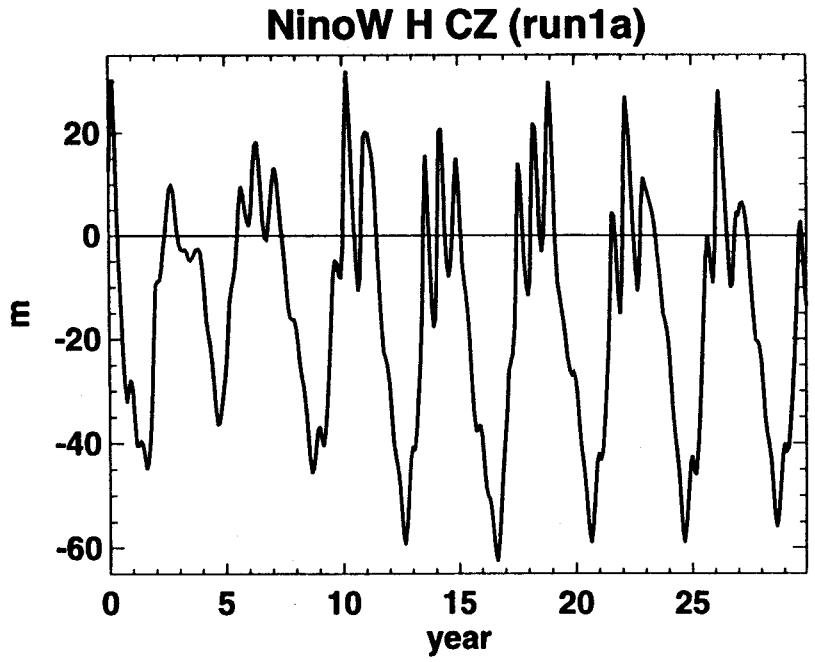
NinoW H CZ (run1a)
m
20
0
-20
-40
-60
0
5
10
15
20
25
year

Fig.3

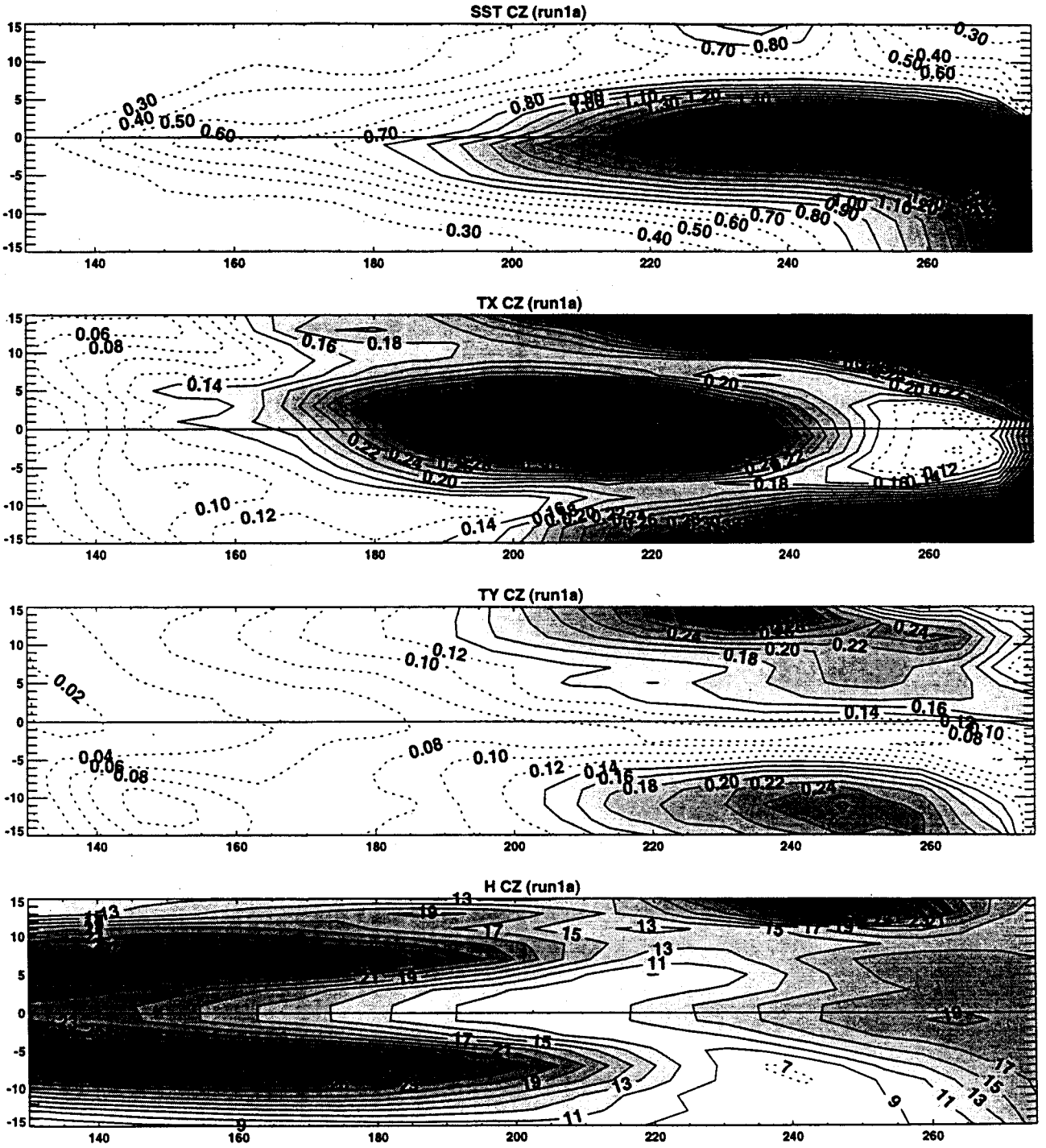

Fig.4

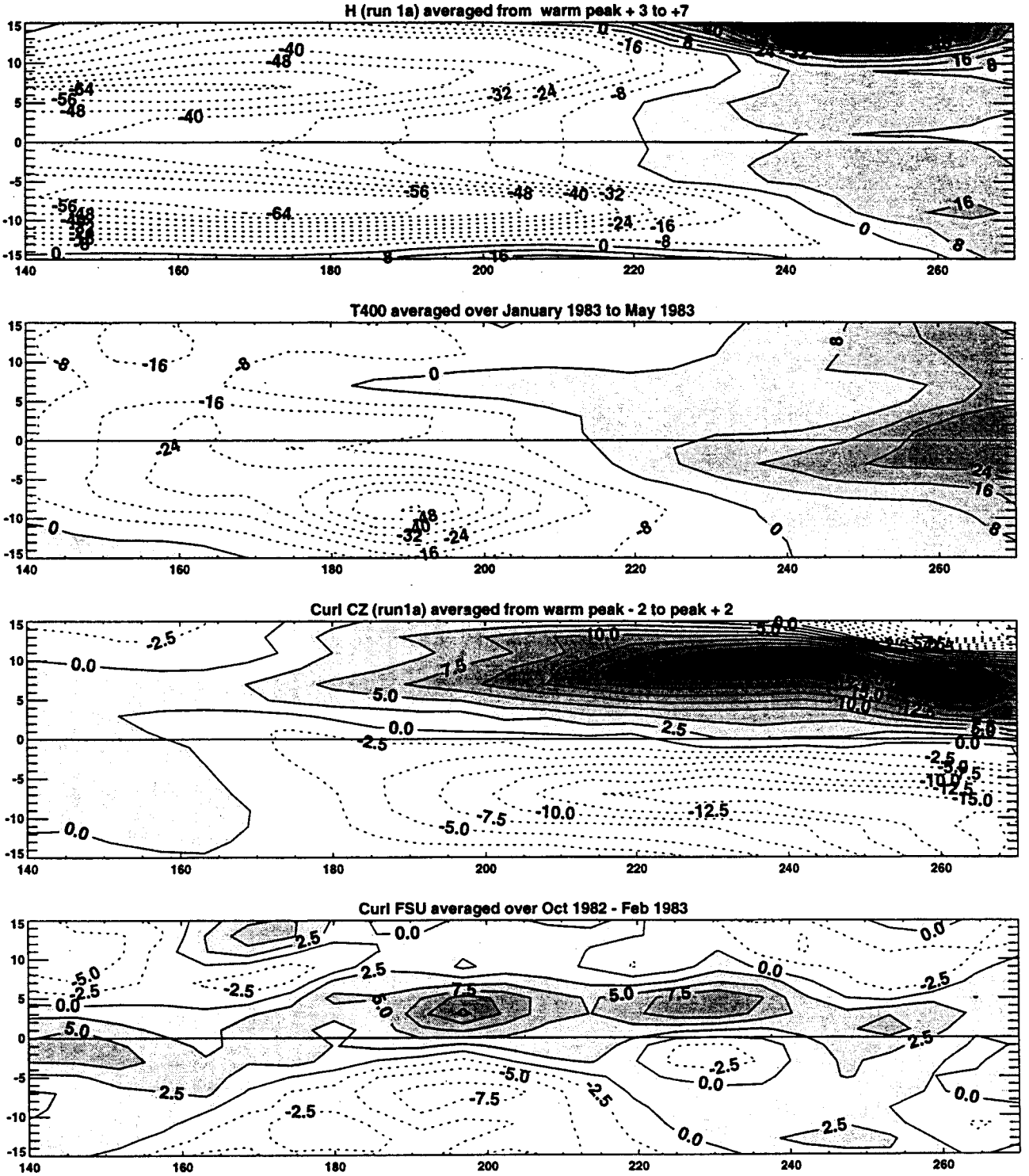
H (run 1a) averaged from warm peak + 3 to +7
T400 averaged over January 1983 to May 1983
Curl CZ (run1a) averaged from warm peak - 2 to peak + 2
Curl FSU averaged over Oct 1982 - Feb 1983

Fig.5

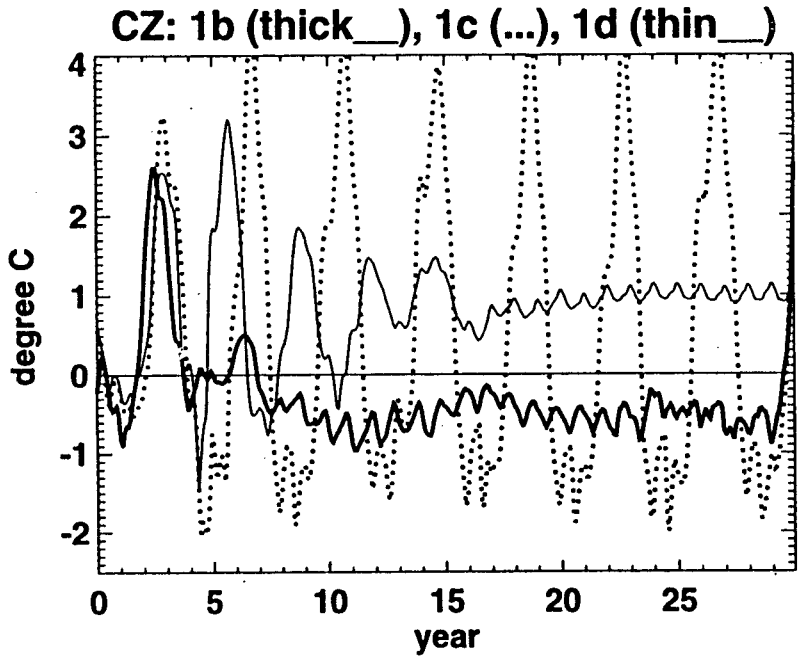
CZ: 1b (thick__), 1c (...), 1d (thin__)
degree C
year
4
3
2
1
0
-1
-2
0
5
10
15
20
25

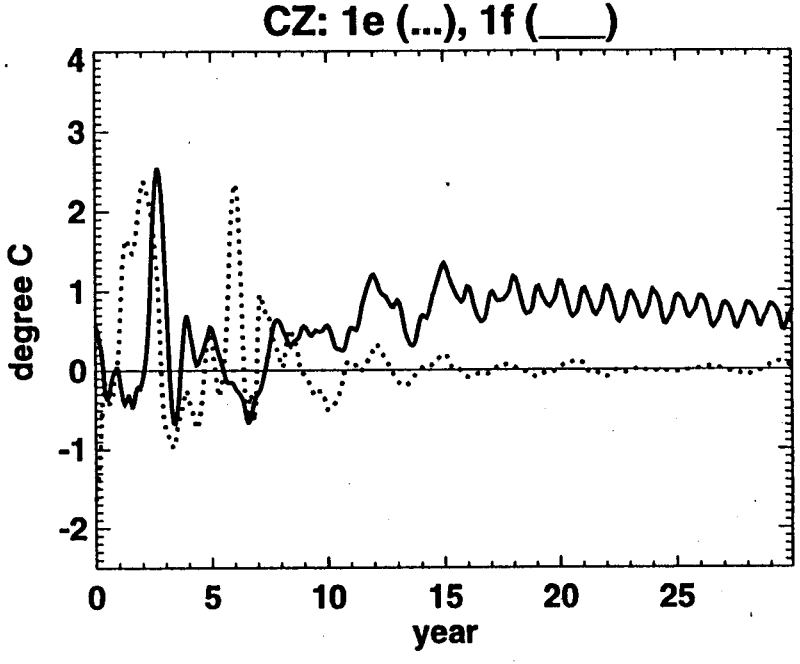
CZ: 1e (...), 1f (___)
degree C
year
4
3
2
1
0
-1
-2
0
5
10
15
20
25

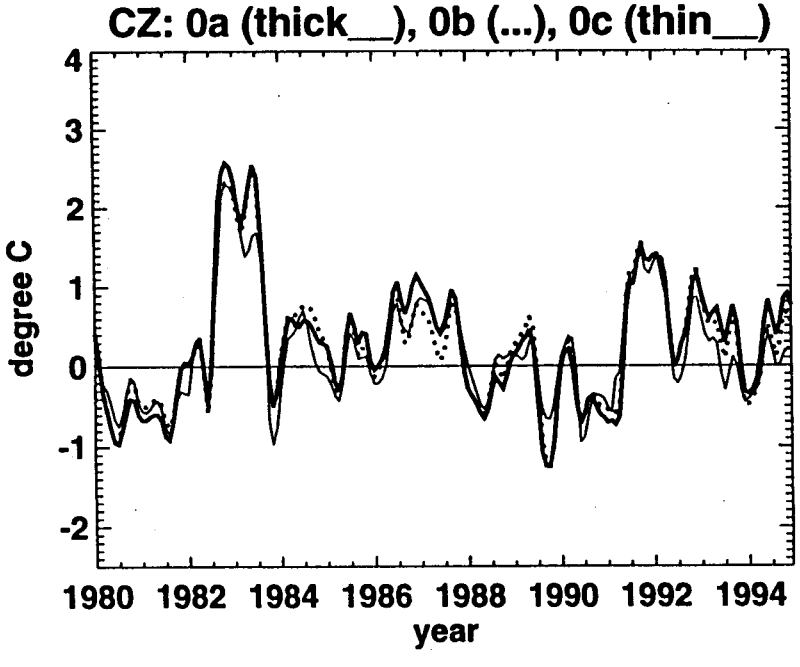
CZ: 0a (thick__), 0b (...), 0c (thin__)
degree C
year
4
3
2
1
0
-1
-2
1980
1982
1984
1986
1988
1990
1992
1994

Fig.6

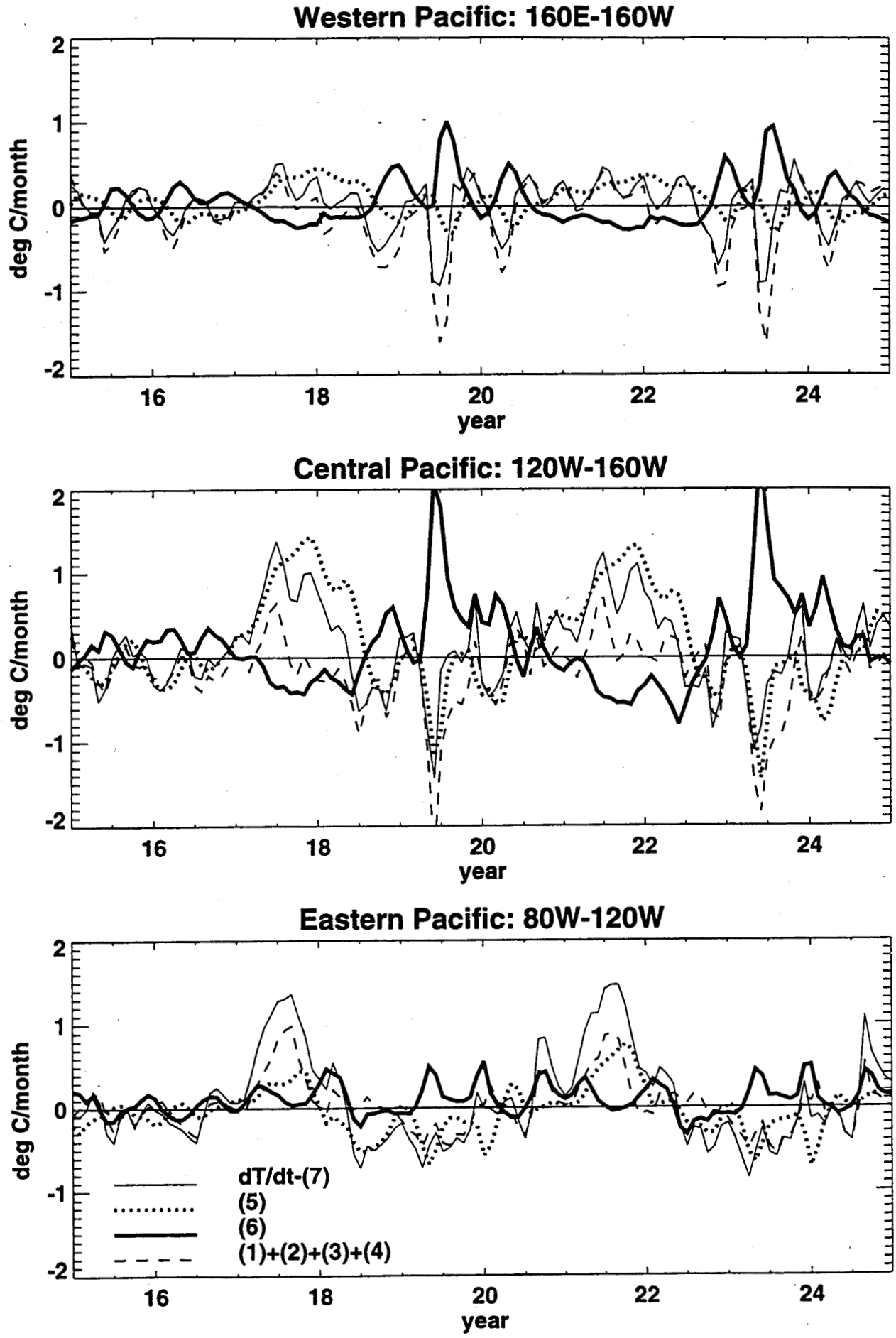
Western Pacific: 160E-160W
deg C/month
year
Central Pacific: 120W-160W
deg C/month
year
Eastern Pacific: 80W-120W
deg C/month
year
dT/dt-(7)
(5)
(6)
(1)+(2)+(3)+(4)

Fig.7

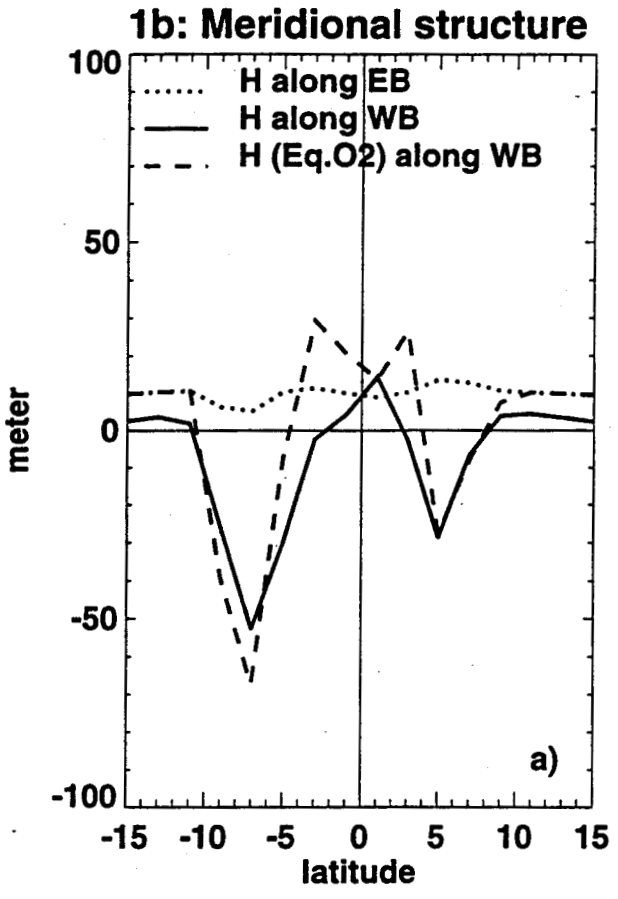
1b: Meridional structure
H along EB
H along WB
H (Eq.O2) along WB
meter
latitude
a)

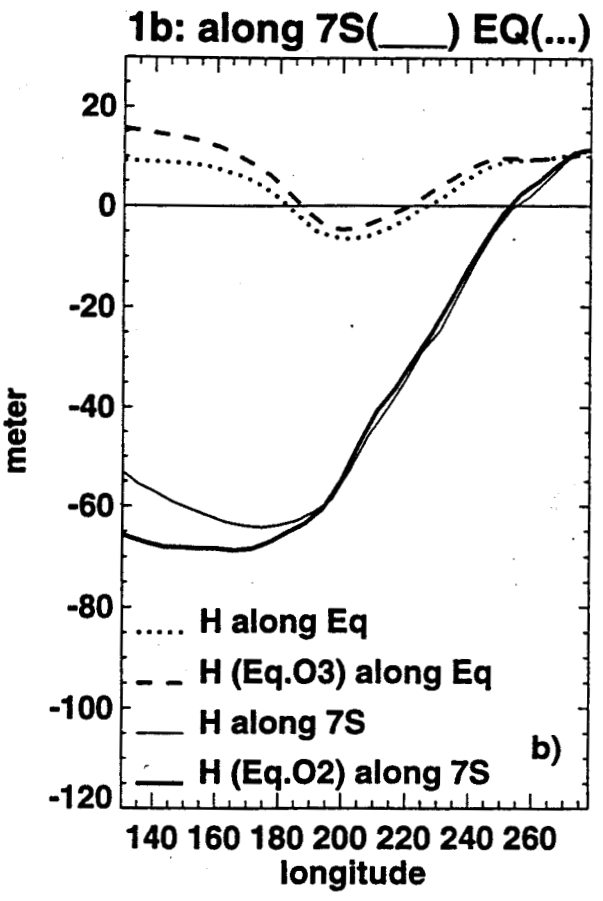
1b: along 7S(___) EQ(...)
H along Eq
H (Eq.O3) along Eq
H along 7S
H (Eq.O2) along 7S
meter
longitude
b)

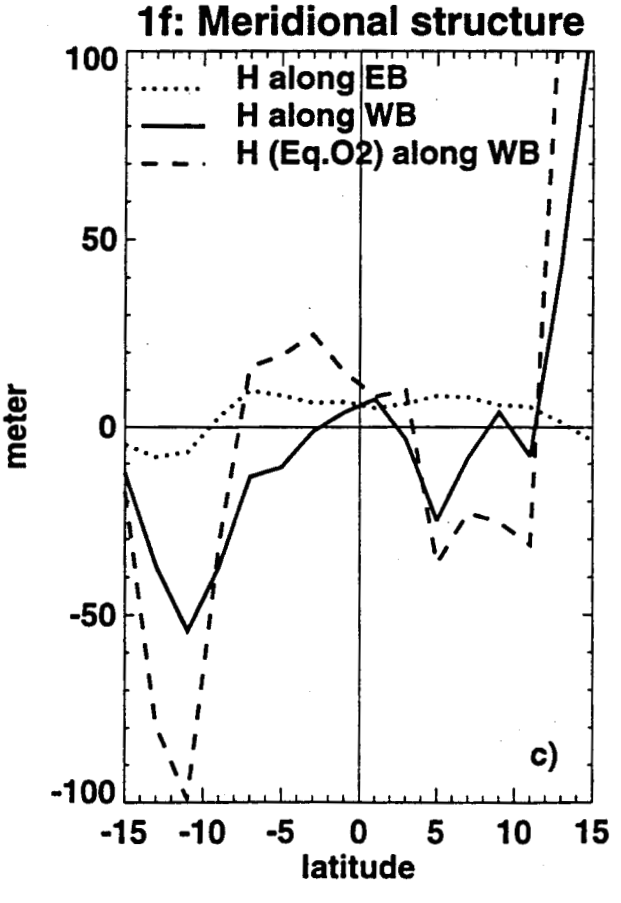
1f: Meridional structure
H along EB
H along WB
H (Eq.O2) along WB
meter
latitude
c)

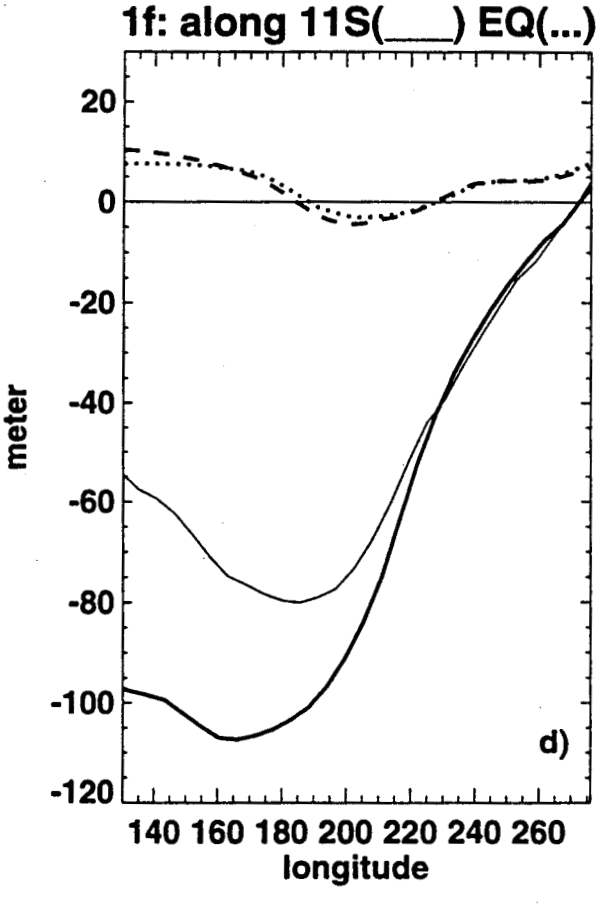
1f: along 11S(___) EQ(...)
meter
longitude
d)

Fig.8ab

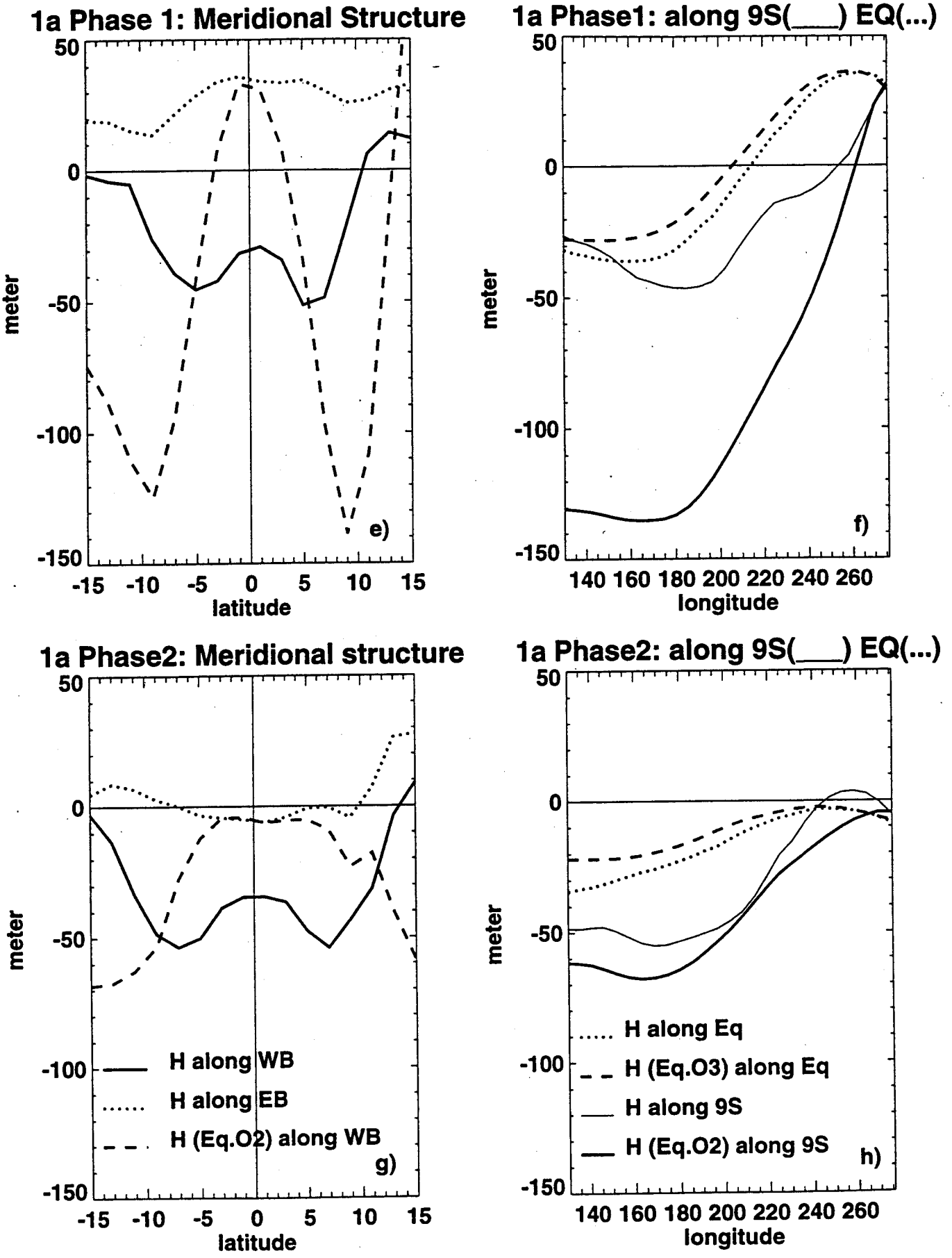
1a Phase 1: Meridional Structure
meter
50
0
-50
-100
-150
-15 -10 -5 0 5 10 15
latitude
e)
1a Phase1: along 9S(___) EQ(...)
meter
50
0
-50
-100
-150
140 160 180 200 220 240 260
longitude
f)
1a Phase2: Meridional structure
meter
50
0
-50
-100
-150
H along WB
H along EB
H (Eq.O2) along WB
-15 -10 -5 0 5 10 15
latitude
g)
1a Phase2: along 9S(___) EQ(...)
meter
50
0
-50
-100
-150
H along Eq
H (Eq.O3) along Eq
H along 9S
H (Eq.O2) along 9S
140 160 180 200 220 240 260
longitude
h)

Fig.8efgh

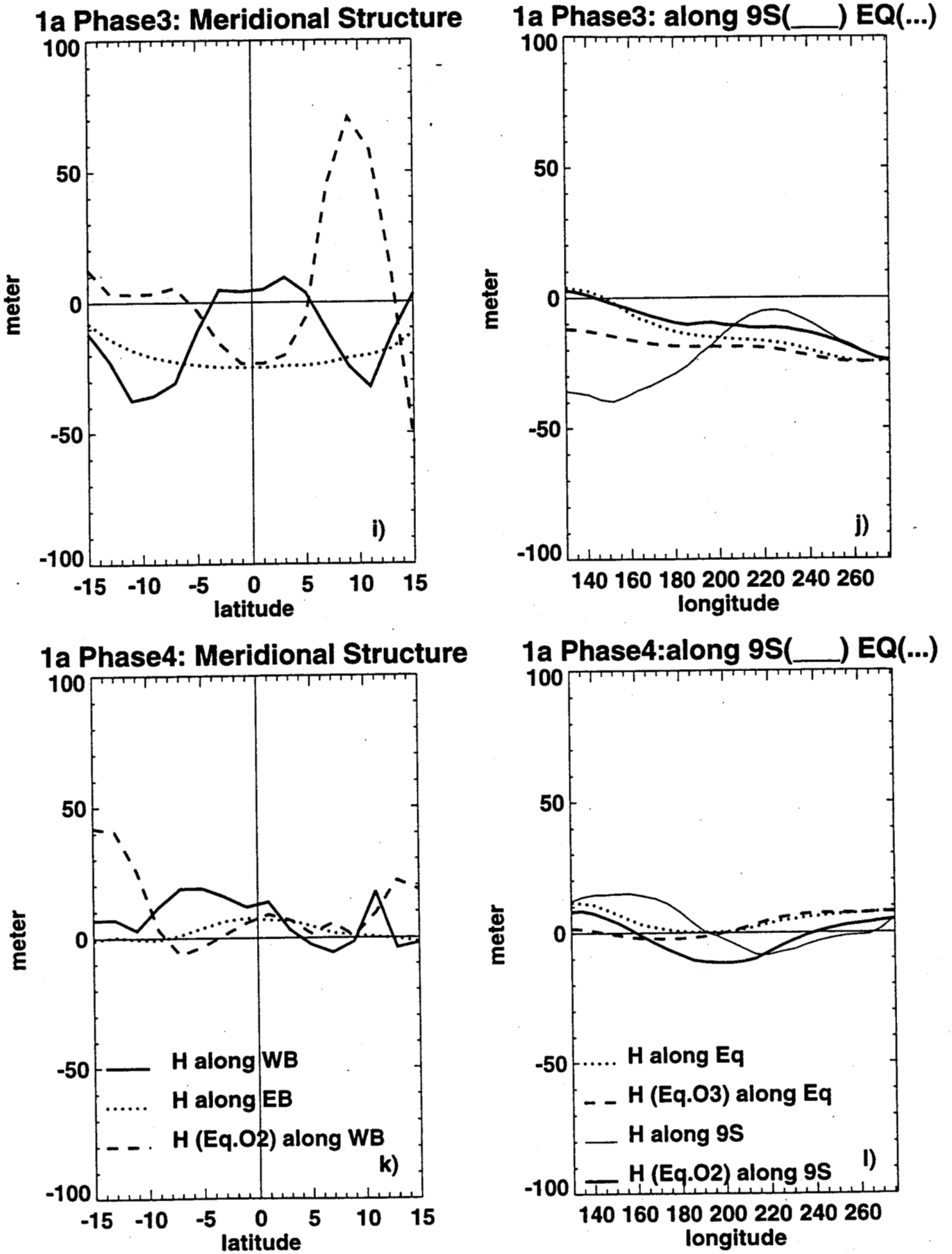
1a Phase3: Meridional Structure
meter
100
50
0
-50
-100
-15 -10 -5 0 5 10 15
latitude
i)
1a Phase3: along 9S(___) EQ(...)
meter
100
50
0
-50
-100
140 160 180 200 220 240 260
longitude
j)
1a Phase4: Meridional Structure
meter
100
50
0
-50
-100
H along WB
H along EB
H (Eq.O2) along WB
k)
-15 -10 -5 0 5 10 15
latitude
1a Phase4:along 9S(___) EQ(...)
meter
100
50
0
-50
-100
H along Eq
H (Eq.O3) along Eq
H along 9S
H (Eq.O2) along 9S
l)
140 160 180 200 220 240 260
longitude

Fig.8ijkl

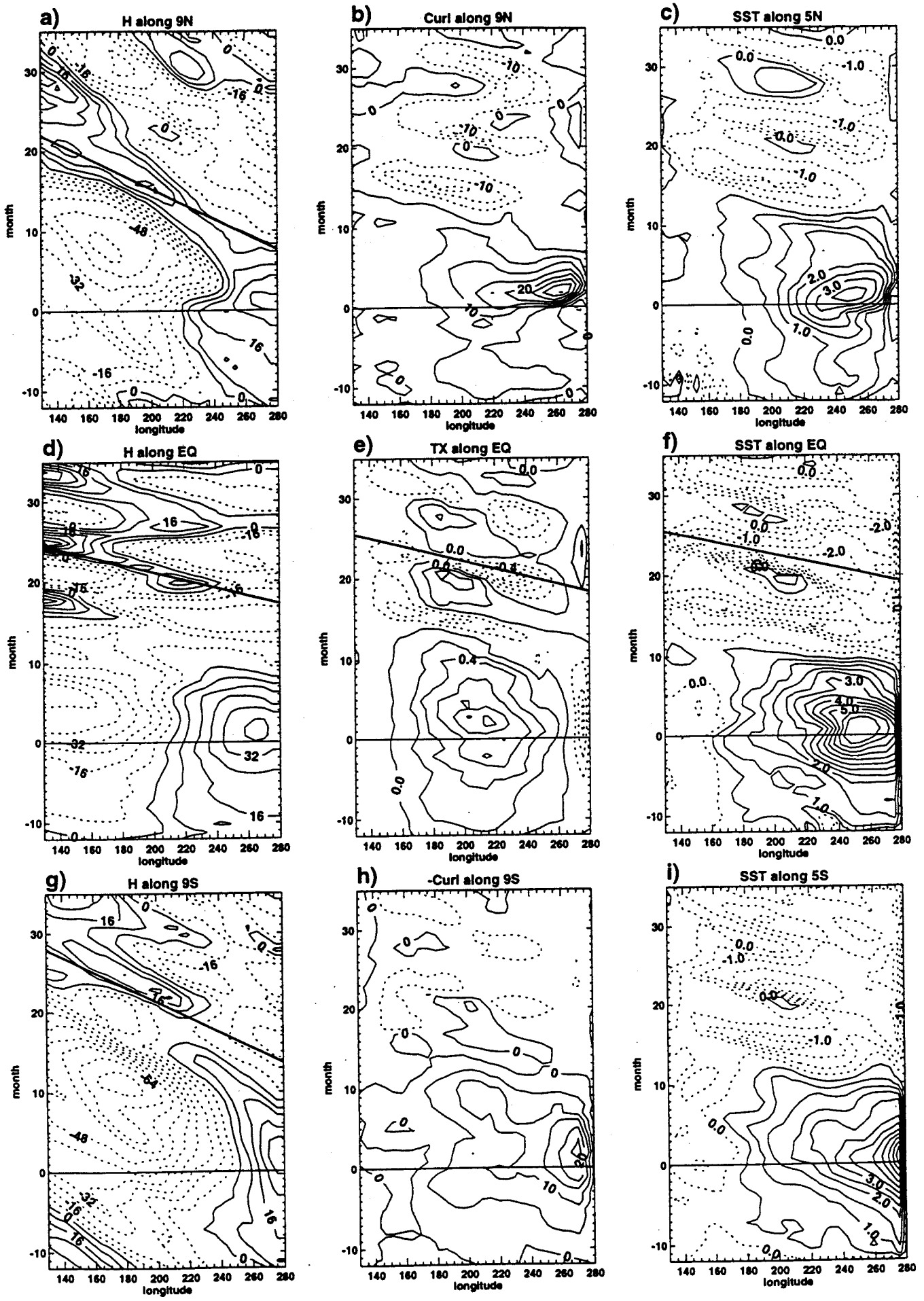
a) H along 9N
b) Curl along 9N
c) SST along 5N
d) H along EQ
e) TX along EQ
f) SST along EQ
g) H along 9S
h) -Curl along 9S
i) SST along 5S
month
longitude

Fig.9

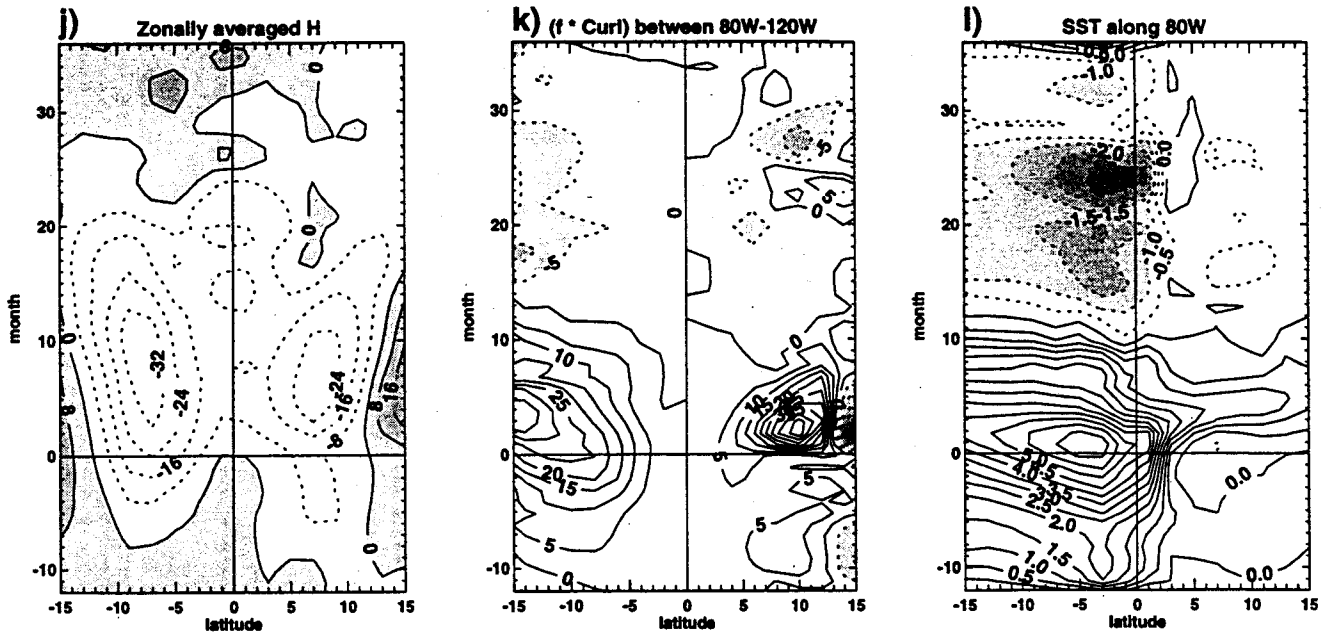
j) Zonally averaged H
k) (f * Curl) between 80W-120W
l) SST along 80W
month
latitude

Fig.9bis

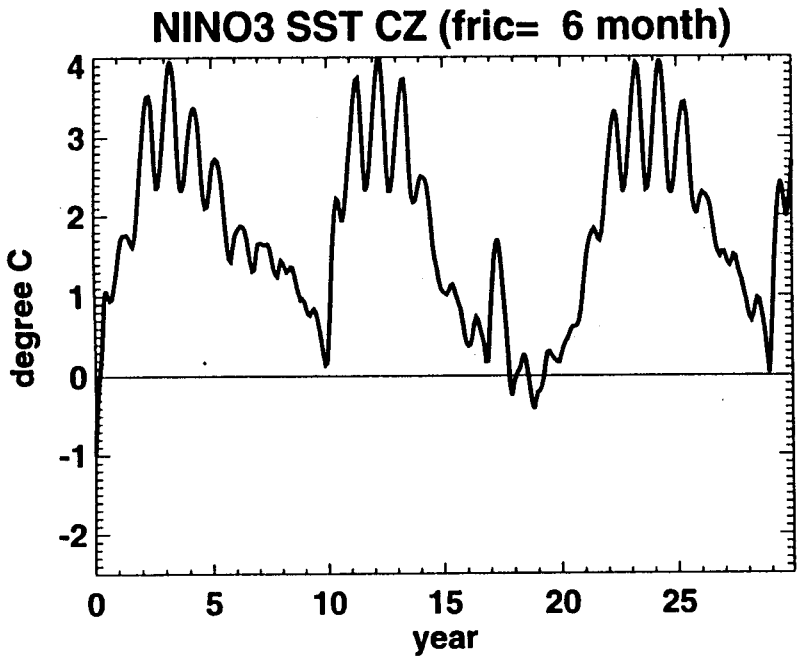
NINO3 SST CZ (fric= 6 month)
degree C
year

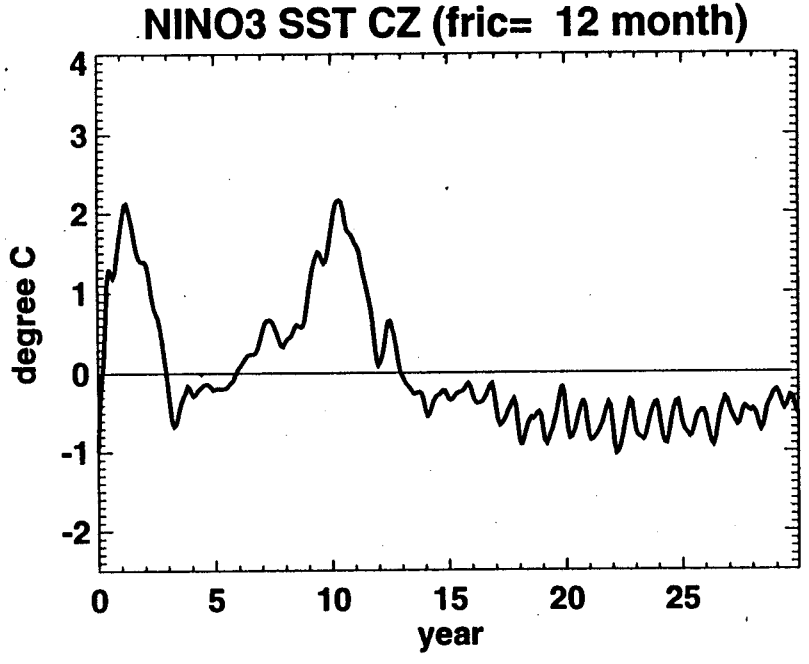
NINO3 SST CZ (fric= 12 month)
degree C
year

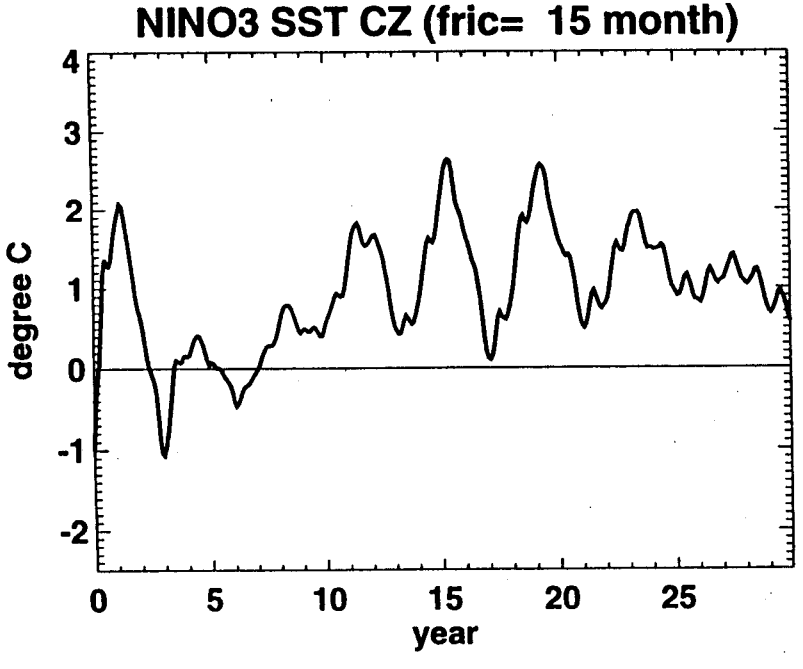
NINO3 SST CZ (fric= 15 month)
degree C
year

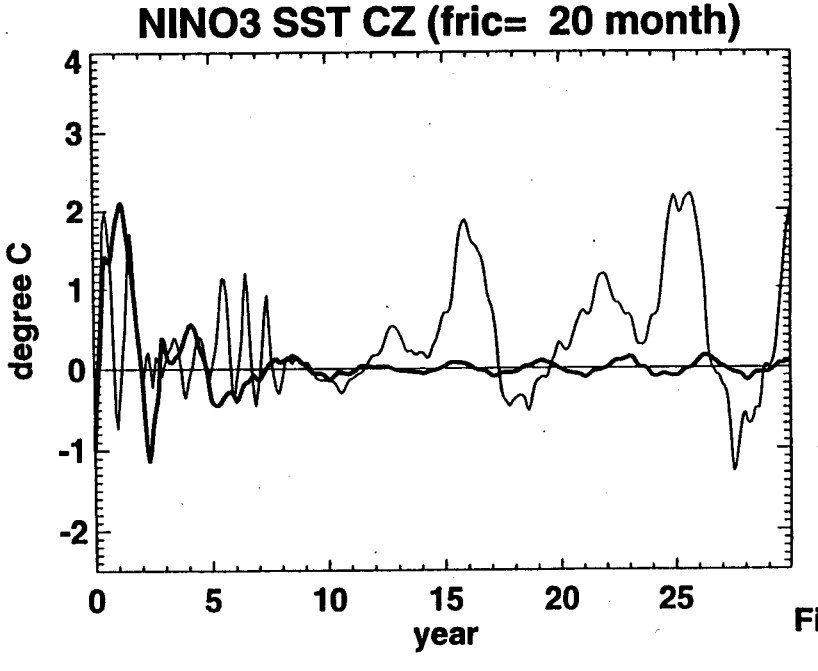
NINO3 SST CZ (fric= 20 month)
degree C
year

Fig.10

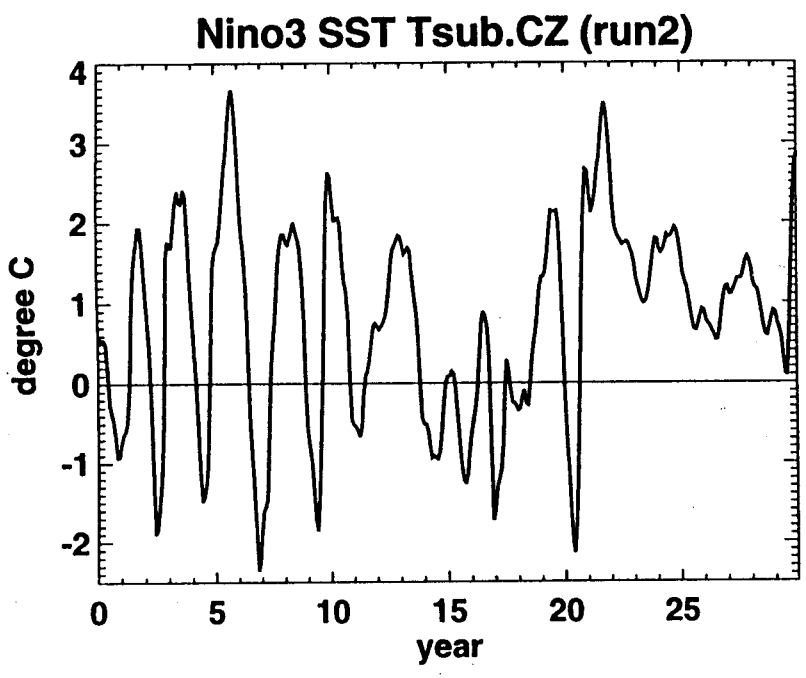
Nino3 SST Tsub.CZ (run2)
degree C
year

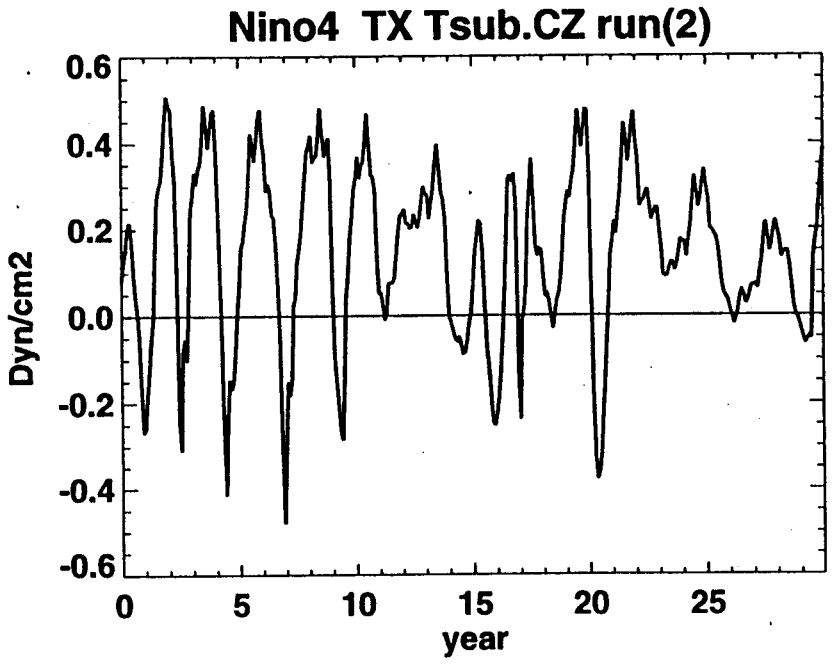
Nino4 TX Tsub.CZ run(2)
Dyn/cm2
year

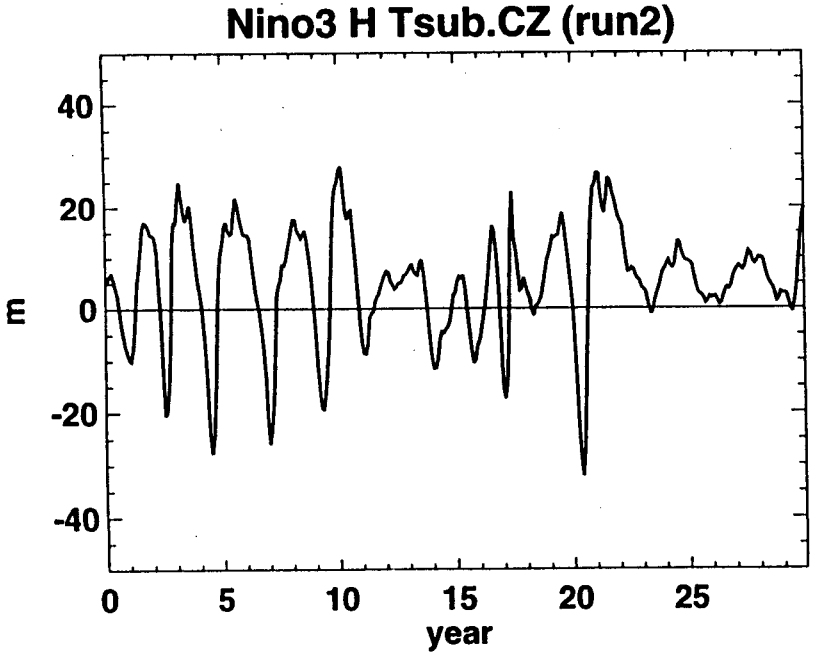
Nino3 H Tsub.CZ (run2)
m
year

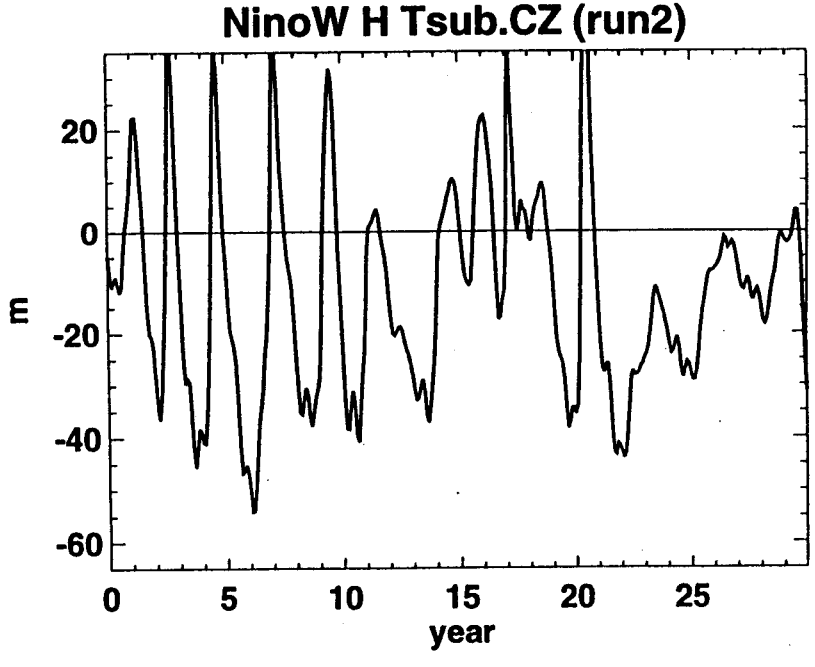
NinoW H Tsub.CZ (run2)
m
year

Fig.11

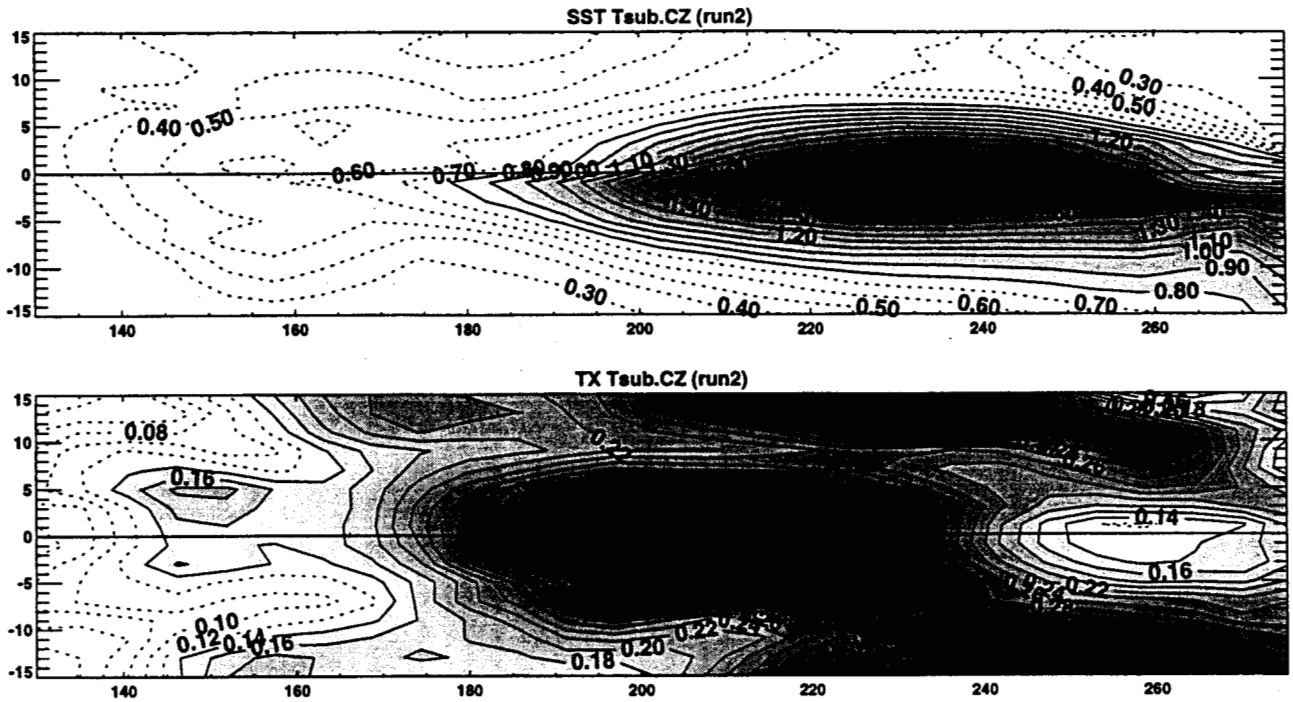

Fig.12

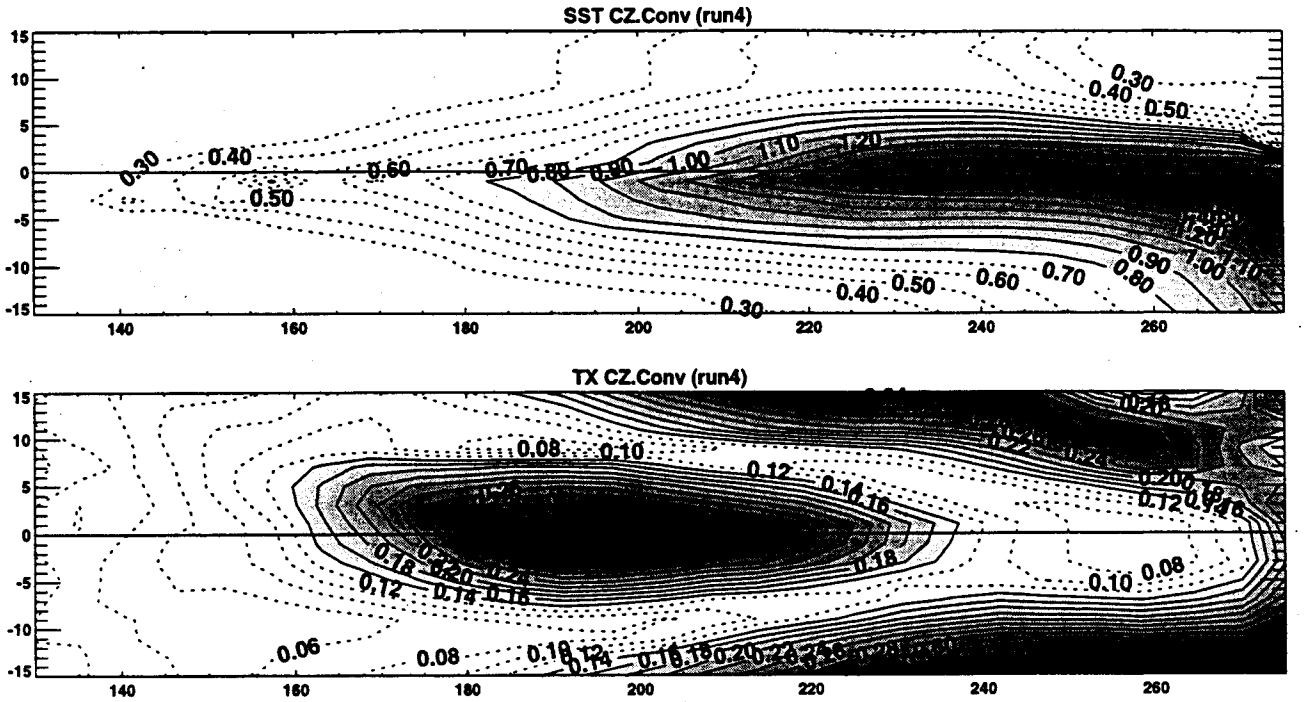
SST CZ.Conv (run4)
15
10
5
0
-5
-10
-15
140
160
180
200
220
240
260
0.30
0.40
0.50
0.60
0.70
0.80
0.90
1.00
1.10
1.20
TX CZ.Conv (run4)
0.06
0.08
0.10
0.12
0.14
0.16
0.18
0.20

Fig.13

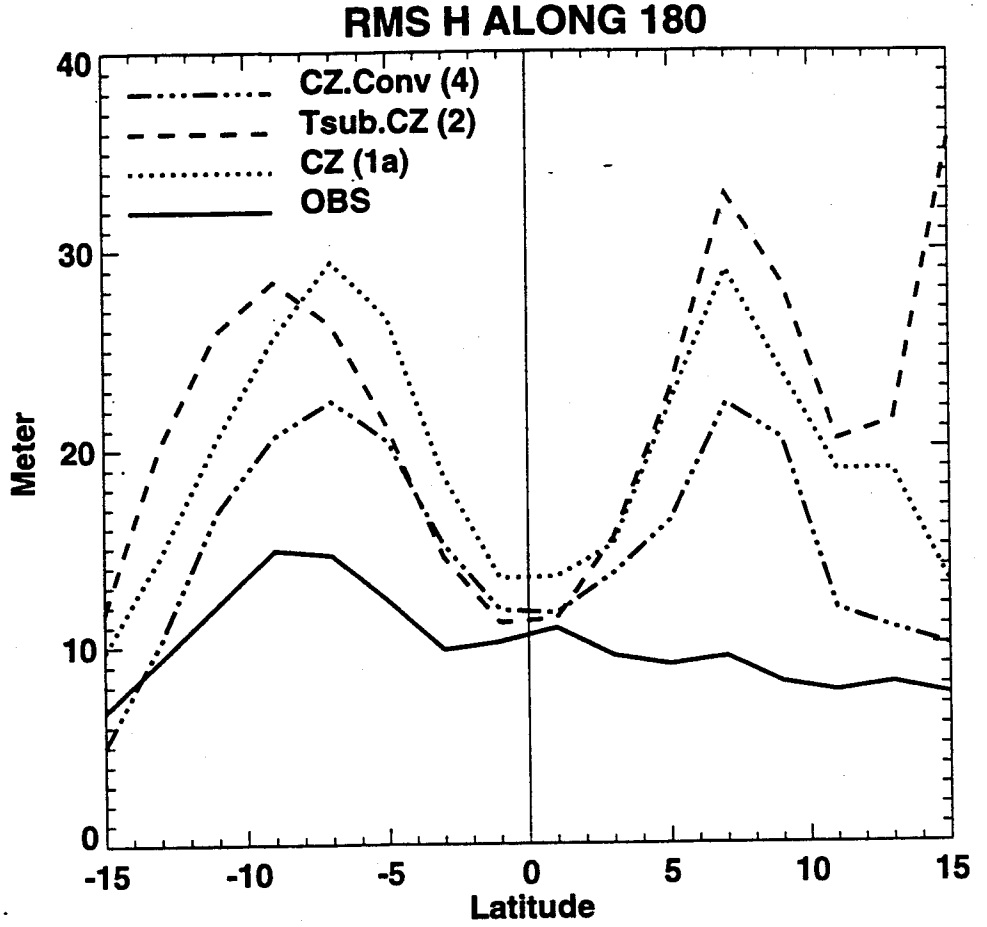
RMS H ALONG 180
CZ.Conv (4)
Tsub.CZ (2)
CZ (1a)
OBS
Meter
40
30
20
10
0
-15
-10
-5
0
5
10
15
Latitude

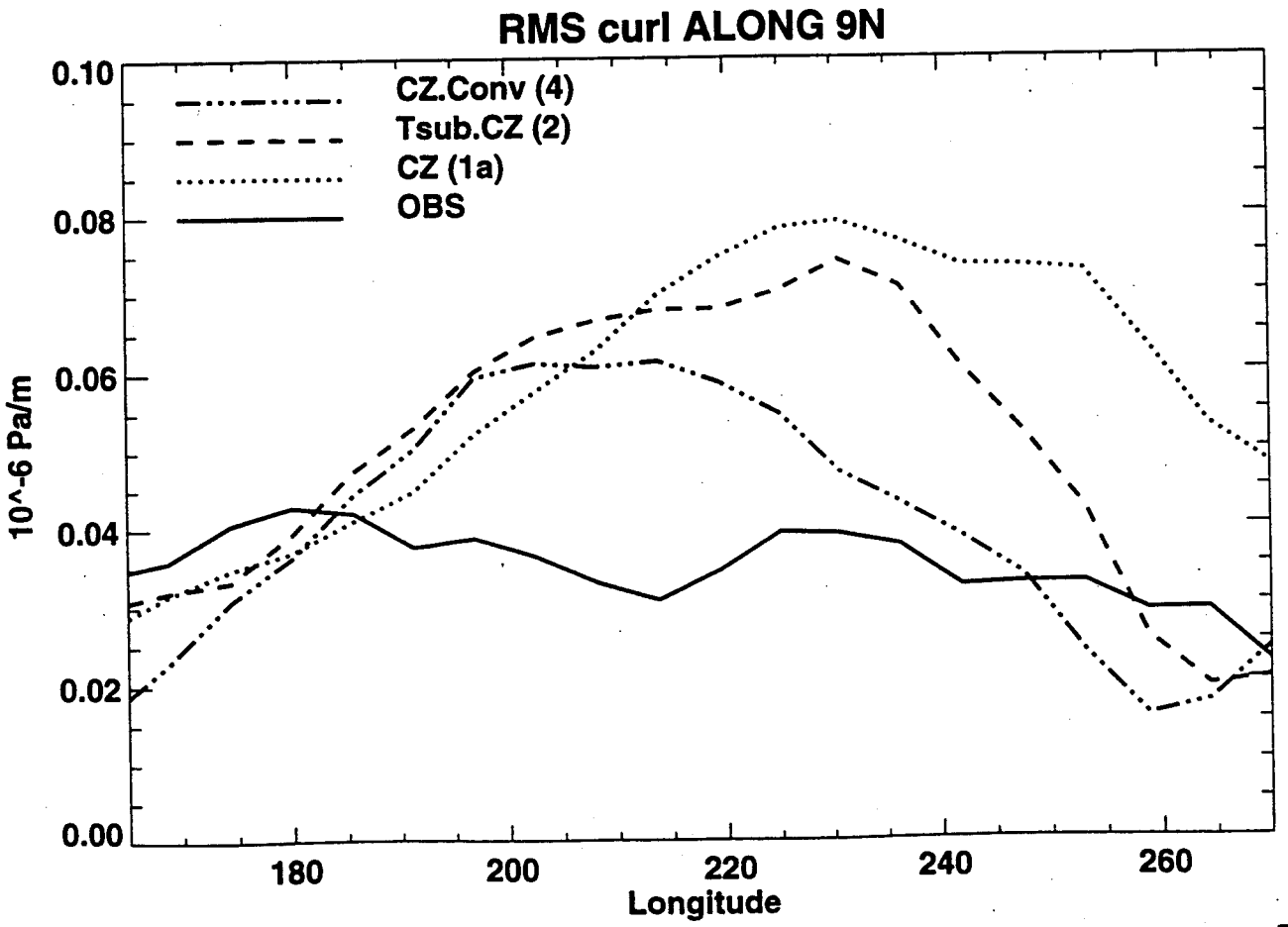
RMS curl ALONG 9N
CZ.Conv (4)
Tsub.CZ (2)
CZ (1a)
OBS
10^-6 Pa/m
0.10
0.08
0.06
0.04
0.02
0.00
180
200
220
240
260
Longitude

Fig.14

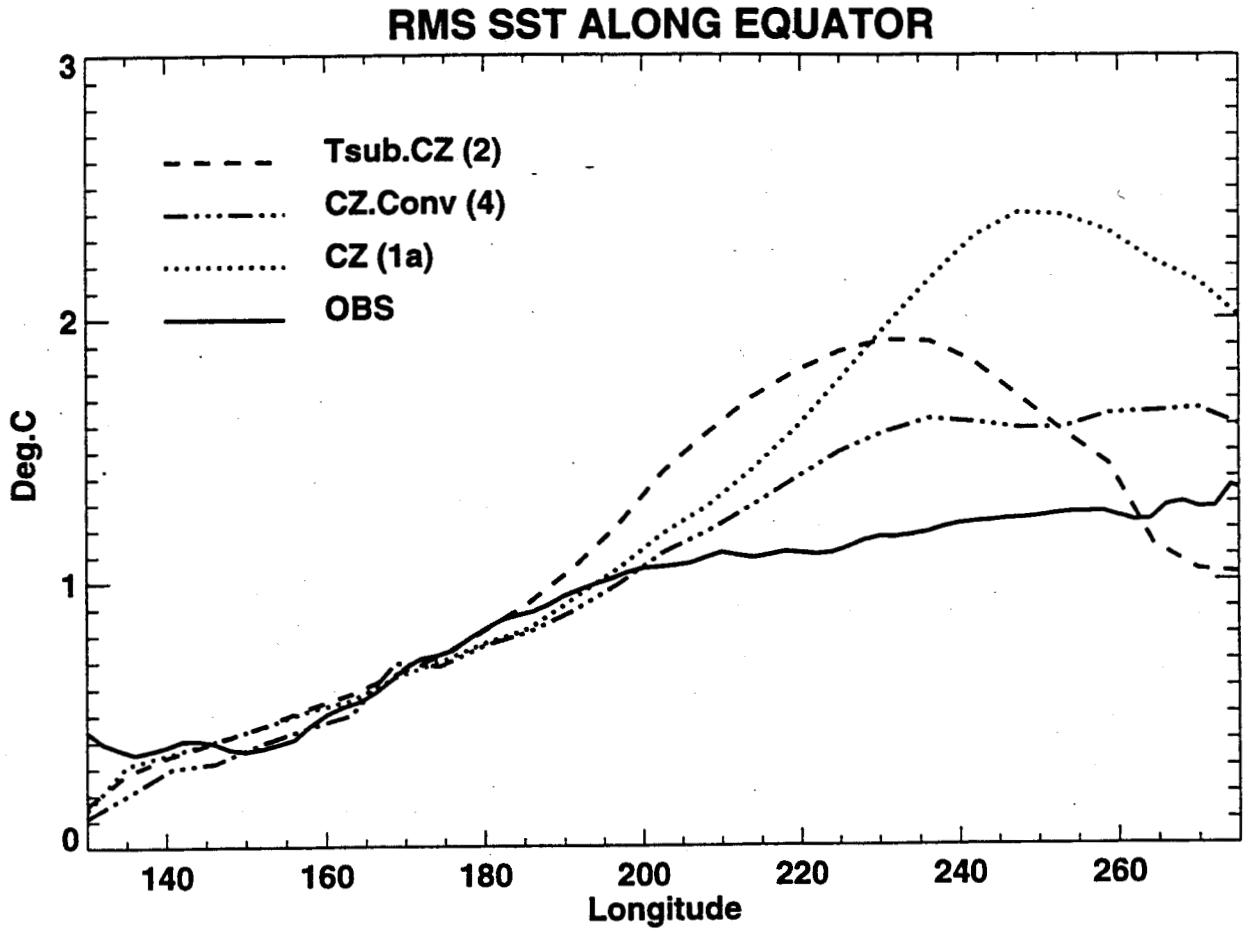
RMS SST ALONG EQUATOR
Tsub.CZ (2)
CZ.Conv (4)
CZ (1a)
OBS
Deg.C
0
1
2
3
140
160
180
200
220
240
260
Longitude

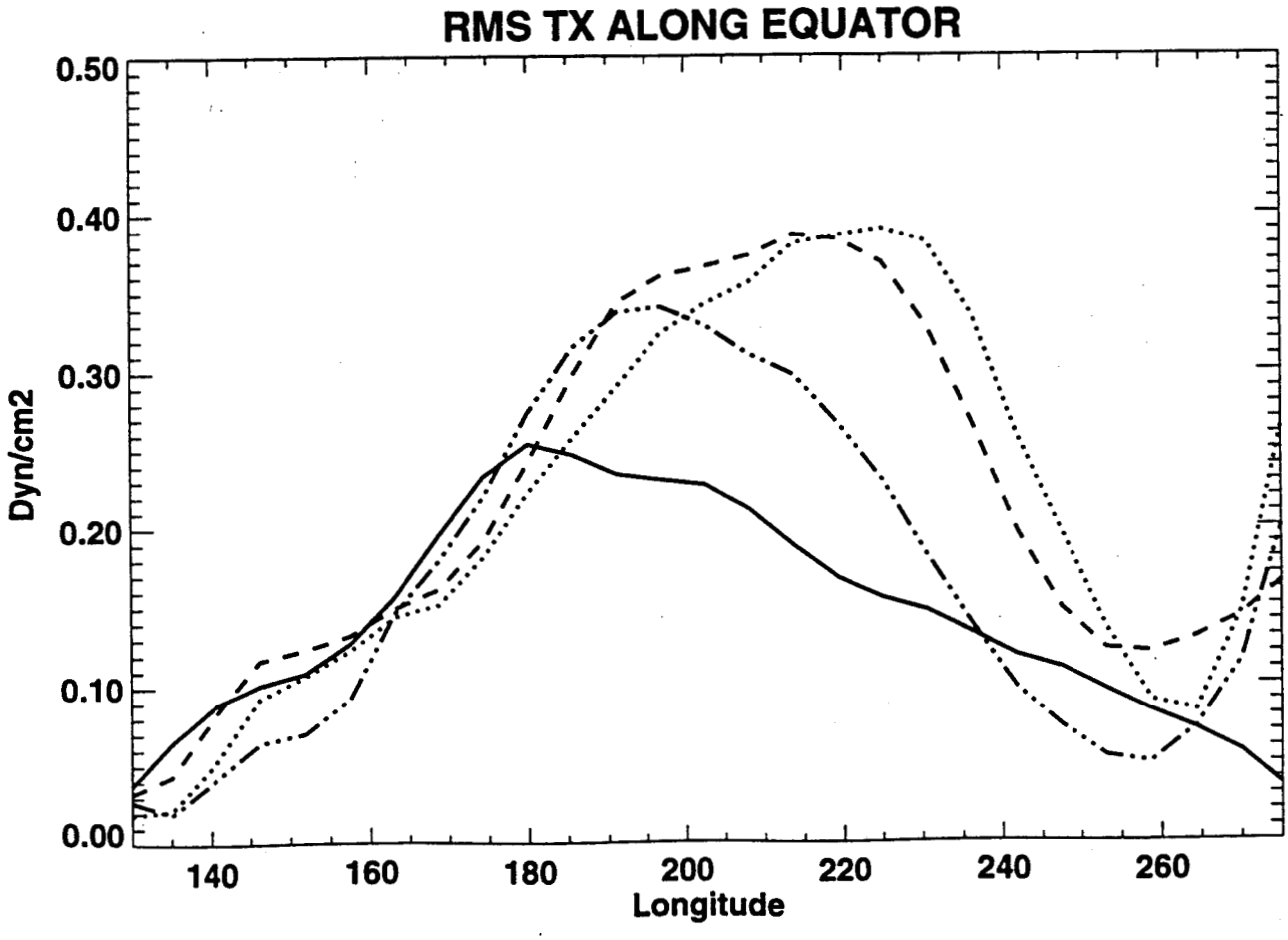
RMS TX ALONG EQUATOR
Dyn/cm2
0.00
0.10
0.20
0.30
0.40
0.50
140
160
180
200
220
240
260
Longitude

Fig.15

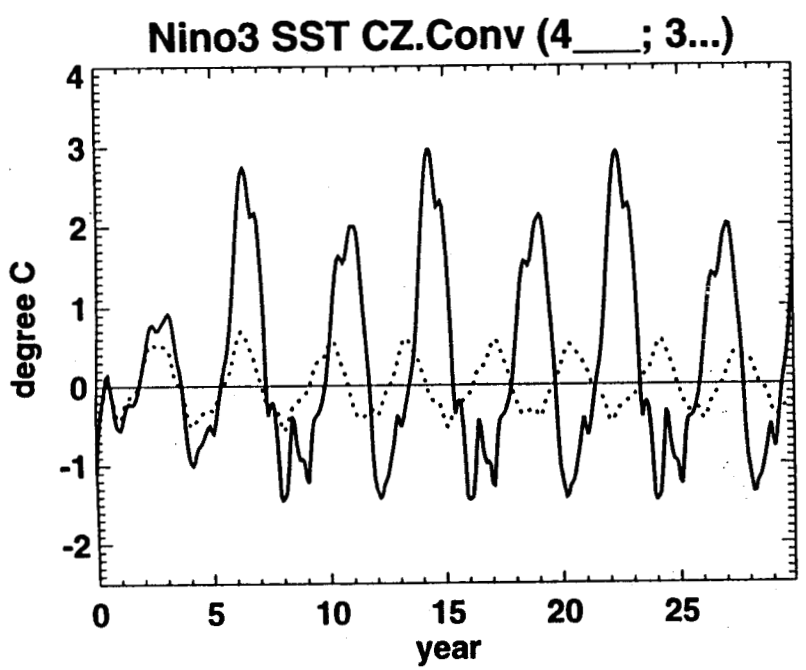
Nino3 SST CZ.Conv (4___; 3...)
degree C
4
3
2
1
0
-1
-2
0
5
10
15
20
25
year

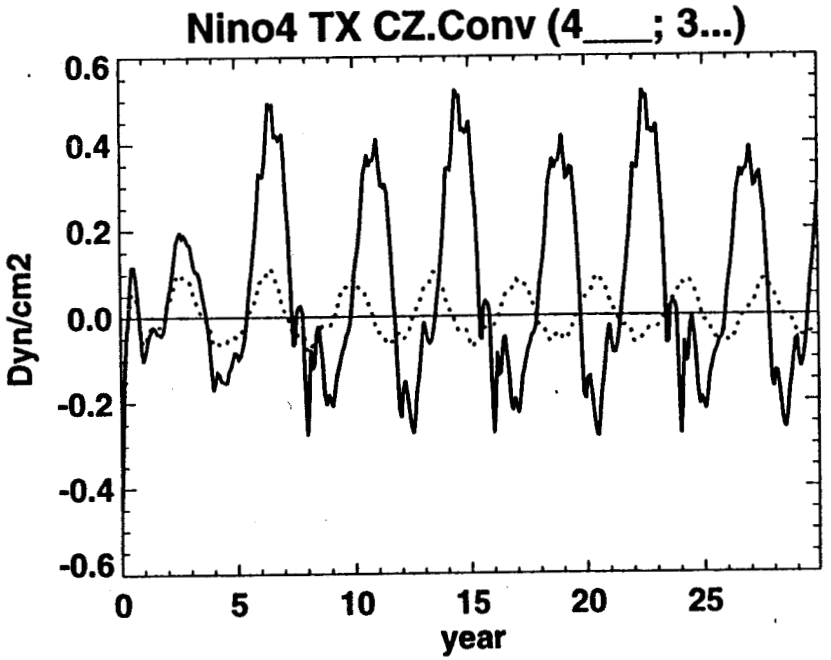
Nino4 TX CZ.Conv (4___; 3...)
Dyn/cm2
0.6
0.4
0.2
0.0
-0.2
-0.4
-0.6
0
5
10
15
20
25
year

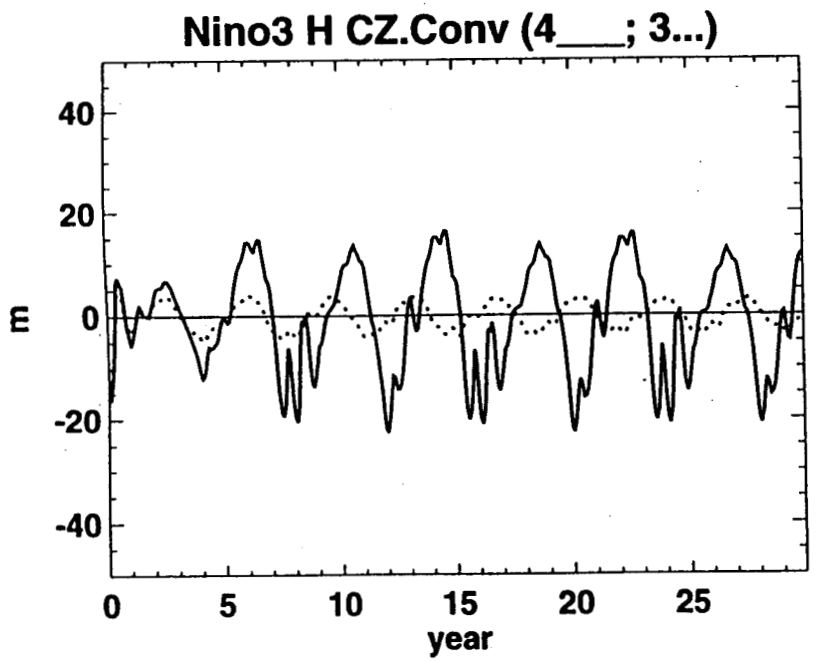
Nino3 H CZ.Conv (4___; 3...)
m
40
20
0
-20
-40
0
5
10
15
20
25
year

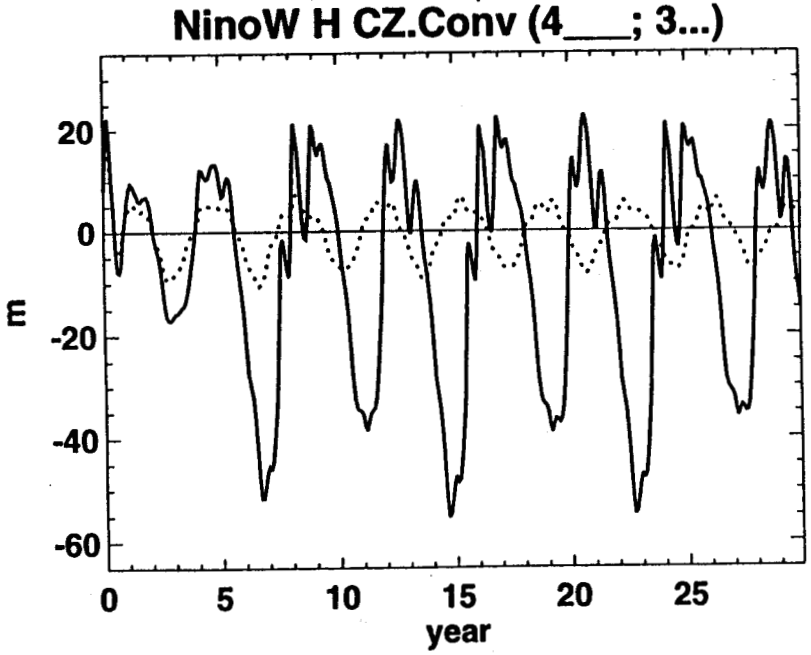
NinoW H CZ.Conv (4___; 3...)
m
20
0
-20
-40
-60
0
5
10
15
20
25
year

Fig.16